2017

STRATIGRAPHIC, GEOCHEMICAL, AND GEOCHRONOLOGICAL ANALYSIS OF THE WOLFCAMP-D INTERVAL, MIDLAND BASIN, TEXAS

Zachary S. Perlman
University of Kentucky, zspe222@uky.edu
Digital Object Identifier: https://doi.org/10.13023/ETD.2017.163

STUDENT AGREEMENT:

I represent that my thesis or dissertation and abstract are my original work. Proper attribution has been given to all outside sources. I understand that I am solely responsible for obtaining any needed copyright permissions. I have obtained needed written permission statement(s) from the owner(s) of each third-party copyrighted matter to be included in my work, allowing electronic distribution (if such use is not permitted by the fair use doctrine) which will be submitted to UKnowledge as Additional File.

I hereby grant to The University of Kentucky and its agents the irrevocable, non-exclusive, and royalty-free license to archive and make accessible my work in whole or in part in all forms of media, now or hereafter known. I agree that the document mentioned above may be made available immediately for worldwide access unless an embargo applies.

I retain all other ownership rights to the copyright of my work. I also retain the right to use in future works (such as articles or books) all or part of my work. I understand that I am free to register the copyright to my work.

REVIEW, APPROVAL AND ACCEPTANCE

The document mentioned above has been reviewed and accepted by the student's advisor, on behalf of the advisory committee, and by the Director of Graduate Studies (DGS), on behalf of the program; we verify that this is the final, approved version of the student's thesis including all changes required by the advisory committee. The undersigned agree to abide by the statements above.

Zachary S. Perlman, Student

Dr. Michael M. McGlue, Major Professor

Dr. Edward Woolery, Director of Graduate Studies

STRATIGRAPHIC, GEOCHEMICAL, AND GEOCHRONOLOGICAL ANALYSIS OF THE WOLFCAMP-D INTERVAL, MIDLAND BASIN, TEXAS

THESIS

A thesis submitted in partial fulfillment of the requirements for the degree of Masters of Science in the College of Arts and Sciences at the University of Kentucky

By

Zachary Seth Perlman

Lexington, Kentucky

Director: Dr. Michael M. McGlue, Pioneer Professor of Earth and Environmental Sciences

Lexington, Kentucky

2017

ABSTRACT OF THESIS

STRATIGRAPHIC, GEOCHEMICAL, AND GEOCHRONOLOGICAL ANALYSIS OF THE WOLFCAMP-D INTERVAL, MIDLAND BASIN, TEXAS

Subsurface data derived from ~388 ft of drill core from Martin County (TX) were used to understand the depositional setting of the Wolfcamp-D, a petroleum producing interval in the Midland Basin. Elemental geochemistry collected via x-ray fluorescence revealed a highly variable depositional history marked by the deposition of diverse siliciclastic and carbonate lithofacies. Integration of multiple datasets resulted in the interpretation of nine lithofacies, whose deposition appears cyclical. Correlations between molybdenum and total organic carbon indicate slow recharge of bottom waters and anoxic/euxinicconditions within the basin. The presence of phosphatic nodules coinciding with siliceous black mudrocks suggested high levels of primary productivity driven by upwelling. High-frequency sea level variability, driven by far-field glaciation and regional paleoclimate, were key controls on both the chemostratigraphy and lithofacies. Along-strike variability is seen throughout the basin due to paleobathymetry, proximity and connections to paleochannels, and localized structures. Rhenium-osmium (Re/Os) geochronology was conducted on siliceous mudrocks with high total organic carbon. A depositional age of 300 ± 18 Ma was obtained, partially confirming previous correlations to shelf biostratigraphic data. Scatter in the Re/Os data is likely due to mixing in the basin or non-hydrogenous Os incorporated into the analysis due to the method of preparation.

KEYWORDS: Mudrocks, Unconventional Petroleum Reservoirs, Chemostratigraphy, Lithofacies, Cyclothems, Re-Os Geochronology

Zachary Seth Perlman

2/25/2017

STRATIGRAPHIC, GEOCHEMICAL, AND GEOCHRONOLOGICAL ANALYSIS OF THE WOLFCAMP-D INTERVAL, MIDLAND BASIN, TEXAS

By

Zac Perlman

Dr. Michael M. McGlue

Director of Thesis

Dr. Edward Woolery

Director of Graduate Studies

February 25th, 2017

TABLE OF CONTENTS

LIST OF TABLES

LIST OF FIGURES

CHAPTER ONE: INTRODUCTION

The Midland Basin is the eastern sub-basin of the Greater Permian Basin (GPB) located in western Texas, and it has experienced a resurgence in attention for its potential as an unconventional petroleum province (Frenzel et al., 1988; Waite and Reed, 2014). Early oil exploration interest within the Midland Basin, and to a further extent the GPB, was focused on conventional plays in the Spraberry and Strawn Formations, which consist of sandstone and platform carbonate reservoir rocks with high porosity (Saller et al., 1994; Hamlin and Baumgardner, 2012). Advances in horizontal drilling technologies and fracturing fluids have resulted in historic production of petroleum from previously unattainable unconventional reservoirs in the Midland Basin (Jacobs, 2013; Gaswirth et al., 2016). By drilling horizontally through intervals of interest and stimulating fractures by injecting fluids under high pressure, permeability can be artificially created in tight shale horizons, and hydrocarbons can be driven to the well bore and extracted to the surface (Fisher and Warpinski, 2012). Unconventional target zones of interest in the Midland Basin are the petroleum source rocks of Pennsylvanian and Permian age, with technically recoverable quantities of ~20 billion barrels of oil and ~16 trillion cubic feet of gas (Gaswirth et al., 2016). Interestingly enough, even with the recognition that unconventional resources of the Midland Basin are economically comparable to those of the Bakken and Three Forks Formations (Williston Basin, North Dakota), there is a paucity of literature in the public domain describing the Paleozoic geology of this depositional system (Jarvie et al., 2007; Gaswirth et al., 2013). This can be explained by two factors: (1) the deeper sections of Paleozoic strata, including the Wolfcamp interval, are poorly exposed in outcrop and this inhibits field studies; and (2) subsurface data sets

are proprietary and held closely by oil and gas companies. Time-equivalent strata outcrop in the Sacramento and Guadalupe Mountains (Texas), but these rocks typically consist of platform carbonates (Soreghan, 1994; Soreghan and Giles, 1999). Because this study focuses on subsurface data, it provides an excellent opportunity to expand the current understanding of the depositional history of the Midland Basin. This aims of this thesis are threefold: (1) to integrate petrophysical, geochemical, and stratigraphic datasets, in an effort to better characterize the unconventional reservoir potential of the lower Wolfcamp (also known as the Wolfcamp-D); (2) to describe a depositional model for the Wolfcamp-D that can be integrated with prior studies at the University of Kentucky (UK) and elsewhere; and (3) to use the Re-Os geochronometer to place initial radioisotopic constraints on the depositional age of the Wolfcamp-D.

A recent publication by the U.S. Geological Survey assessed the technically recoverable resources in place for the Wolfcamp Formation (Gaswirth et al., 2016). This report split the formation into the Wolfcamp A, B, C, and D sub-intervals. Basal deposits of the Wolfcamp interval are mainly siliciclastic mudrocks interlayered with calcareous beds, but become more calcareous mudrocks interbedded with carbonates moving up-section (Hamlin and Baumgardner, 2012). Estimated recoverable resources for the Wolfcamp-D are in the range of ~4,000 billion cubic feet of gas, ~5,000 million barrels of oil, and ~400 million barrels of natural gas liquids (Gaswirth et al., 2016). Hydrocarbon recovery for the GPB has increased during the last several years, with production predominantly coming out of the Spraberry, Wolfcamp, and Bone Spring Formations. Production was initially at ~140,000 barrels per day (bbl/d) in 2007, but it has since increased to ~600,000 bbl/d in 2013 (Budzik and Perrin, 2014). Recent

advancements in completion technologies have allowed operators to increase productivity in wells despite a reduction in new wells being drilled and a decline in the peak commodity price experienced in the so-called "shale boom" (Energy Information Administration, 2016).

This study focuses on the Wolfcamp-D (WC-D) of the Midland Basin, the deepest and presumably oldest sub-interval of the Wolfcamp Formation. Shale reservoirs in the A, B, and C intervals are distinctly thicker than those of the WC-D, and hydrocarbon production from those units has been significant; more information exists on those younger Wolfcamp intervals in the public domain. Evidence presented by Horak (1985) suggests that the upper Wolfcamp intervals were deposited during a time period of high rates of basin subsidence (Horak, 1985). Even though there is little information available on the WC-D, the few completed studies provide preliminary insights on the stratigraphy and sedimentology of this interval. The WC-D forms a wedge of mostly siliciclastic sediment, thinning to the north and west. The dominant sources of detrital sediment are located to the south and east of the Midland Basin (Figure 1.1; Frenzel et al., 1988). The stratigraphy of the WC-D is variable depending on the location in the basin. Siliciclastic mudrocks are located within the deepest parts of the basin axis, whereas carbonates are more prevalent along the distal fringes and margins (Hamlin and Baumgardner, 2012). Yet very little else is known about the WC-D.

An important unanswered question relates to the effect of sea level change on the depositional history of the WC-D. The WC-D is thought to be Late Pennsylvanian (299-309 Ma) in age, based on regional correlations made to shelf fusulinid biostratigraphy and limited conodont biofacies data (Waite et al., 2015; Kohn et al., 2016). During the

late Pennsylvanian, high-frequency sea level change was ubiquitous (Isbell et al., 2012; Montañez and Poulsen, 2013). If the WC-D is ~299-309 Ma, how did the varying sea level influence depositional patterns and stratigraphy? Late Pennsylvanian strata of North America and Europe are well known for cyclical patterns of deposition within sediments ("cyclothems"), and has focused on platform carbonates or mixed siliciclastic/carbonate ramps (Saller et al., 1999; Heckel, 2008; Eros et al., 2012), but this research focuses on the potential of the WC-D to contain deep basin cyclothems. Building off of the previous work of Baldwin (2016) and Ryan (2016), this study aims to test how stratal patterns vary along the strike of the Midland Basin, as well as how stacking patterns differ moving up section.

The primary hypothesis motivating this study is that the stratigraphy of the WC-D interval from Martin County (TX) was primarily dictated by glacioeustatic sea level change and global climate conditions of the Late Pennsylvanian. The analytical effort needed to test this hypothesis was diverse and integrative. Lithostratigraphic, petrophysical, geochemical, and sedimentological analyses were completed, in order to develop a broad spectrum of data. Combining these datasets resulted in the interpretation of unique lithofacies types based on physical sedimentological and geochemical characteristics. After lithofacies were identified, stacking patterns and vertical changes in facies abundances were interpreted for the WC-D. The variability in lithofacies through time provides clues on the effects of environmental gradients (e.g., climate, sea level) on deposition. Further insights were made available through inorganic geochemical analyses, which can be used to infer bottom water redox conditions and recharge rates of the Midland Basin seaway during deposition, an important consideration in resolving the

depositional environment and the characterization of potential unconventional petroleum reservoirs. Previous studies (Waite et al., 2015) have inferred that the WC-D was deposited during the Late Pennsylvanian based on well log correlations to shelf fusulinids. This study aims to test this hypothesis regarding the age of the WC-D using the Re-Os geochronometer. Cyclothems across North America have been studied extensively (Heckel, 1986; Veevers and Powell, 1987; Ettensohn et al., 1988; Boardman and Heckel, 1989; West et al., 1997), but the expression of deep basinal cyclothems remains only partly understood. By using this holistic approach, a better understanding of the stratigraphic development within the WC-D of the Midland Basin can be developed. This knowledge is then applied to the unconventional reservoir characterization of the Martin County core. Pioneer Natural Resources, as well as other petroleum exploration companies, is interested in the possibility of developing the WC-D as an unconventional play (Jacobs, 2013; Waite et al., 2015). Comprehensive knowledge of the WC-D will assist in the exploration and production of this interval.

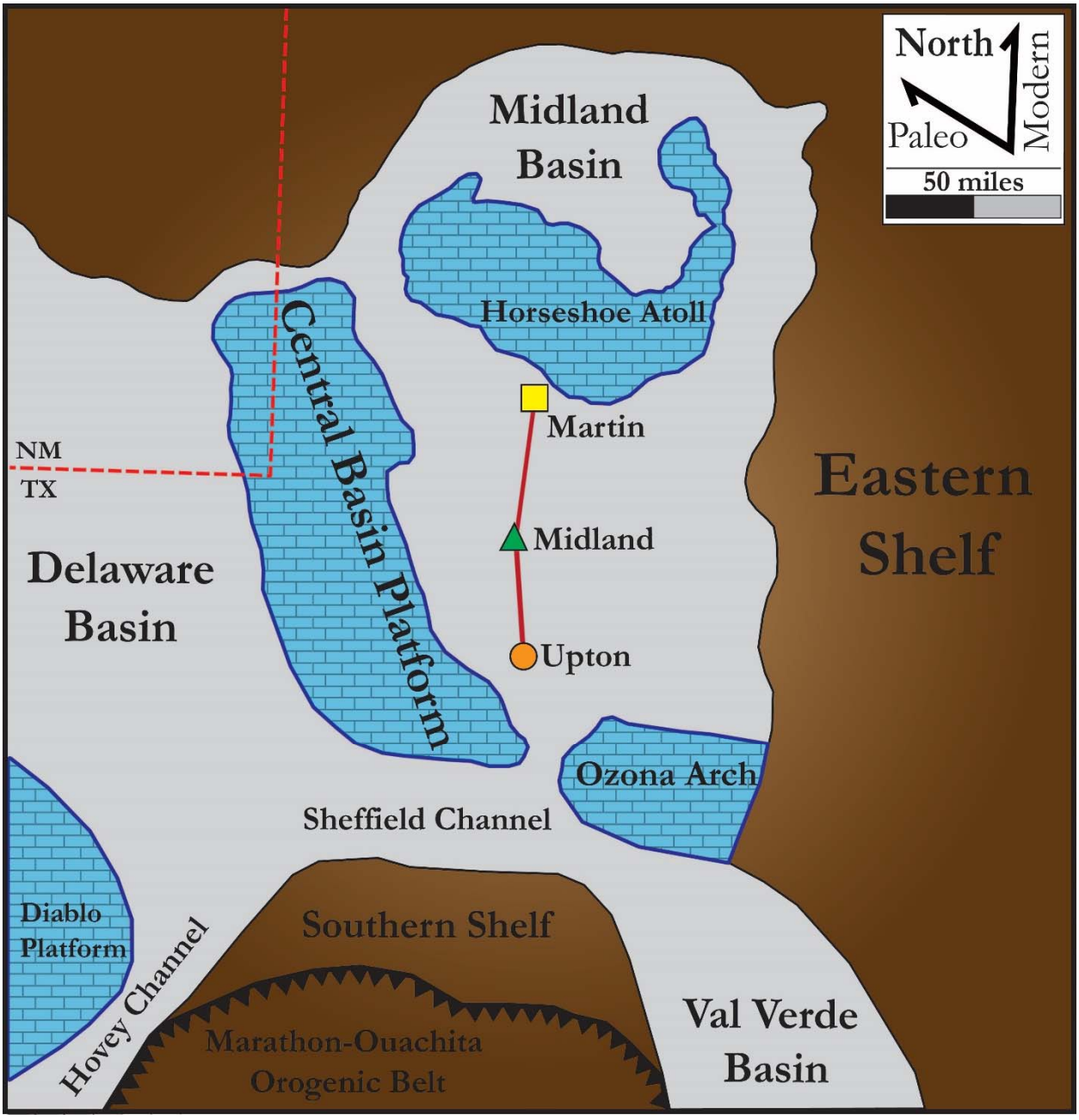

Figure 1.1. Schematic map of the Midland Basin.
Regional conceptual map showing the locations of drill cores donated by Pioneer Natural Resources, as well as geologic features that may have impacted deposition of the WC-D interval. Important features in the basin include the Central Basin Platform, Horseshoe Atoll, Eastern Shelf, and Ozona Arch. The Midland Basin is connected to the Delaware Basin and the rest of the Greater Permian Basin via the Sheffield and Hovey Channels. The focus of this study is the Martin County core, located in the northern axis of the basin. Blue bricks, carbonate environments. Brown shading, mixed siliciclastic environments.

CHAPTER TWO: BACKGROUND

2.1 Tectonic Setting

The extent of the Greater Permian Basin is approximately 297,000 km^2, and it is situated in the southwestern part of the North American craton, straddling west Texas and southeastern New Mexico (Galley, 1958; Frenzel et al., 1988; Yang and Dorobek, 1995). It consists of the relatively deeply subsided Delaware Basin to the west and the shallower Midland Basin to the east. The two sub-basins are separated by the Central Basin Uplift, a carbonate reef system that later evolved into the Central Basin Platform (CBP) (Figure 1.1). The Permian Basin is bordered by the Marathon-Ouachita Foldbelt along its southern margin. The Bend Arch marks the eastern boundary of the Permian Basin and extends northwards from the Llano Uplift, a Precambrian dome structure (Frenzel et al., 1988). The western edge of the Permian Basin is delineated by the Diablo Platform. The Midland Basin is connected to the Delaware Basin via the Sheffield Channel, just south of the Central Basin Platform. The Hovey Channel connects the Delaware Basin to the Panthalassic Ocean (Galley, 1958; Frenzel et al., 1988). Underneath the Permian Basin lies the relict Tobosa Basin, a semi-circular structural sag that formed during the Precambrian (Frenzel et al., 1988).

The Midland Basin is situated on the eastern side of the Permian Basin (Figure 1.1). It exhibits an asymmetric basin morphology, with the broad Eastern Shelf to the east and a steeper margin formed by the Central Basin Platform to the west. The Horseshoe Atoll, a positive-relief carbonate bioherm, is found at the northern end of the basin (Figure 1.1). The elongate basin is approximately 305 km long in the strike direction and 110 km along the dip orientation (Hamlin and Baumgardner, 2012). The Matador Arch

and Palo Duro Basin bound the Midland Basin along its northern border (Mazzullo and Reid, 1989). The Eastern Shelf is comprised of prograding deltaic fan complexes interbedded with carbonate platform lithologies (Frenzel et al., 1988; Mazzullo and Reid, 1989). The southern border of the Midland Basin is bounded by the Ozona Arch, a site of active carbonate deposition during the Late Pennsylvanian-Early Permian (Shumaker, 1992). The Ozona Arch and the Central Basin Platform were both reef-topped carbonate platform uplifts that formed as a result of the Ouachita-Marathon orogeny during the Late Mississippian (Shumaker, 1992).

The Midland Basin, and to a larger extent the Greater Permian Basin, has undergone multiple periods of uplift and subsidence throughout its history (Horak, 1985; Frenzel et al., 1988; Shumaker, 1992). Figure 2.1 shows the timing and movement of Precambrian strata relative to modern-day sea level (Horak, 1985; Ryan, 2016). From the Late Proterozoic to the Mississippian, the Tobosa Basin existed as a shallow sag that underwent passive subsidence (Frenzel et al., 1988; Atchley et al., 1999). During the Late Mississippian, the Marathon-Ouachita Orogeny resulted in the differentiation of the Tobosa Basin into the Midland and Delaware Basins. The reactivation of Early Paleozoic basement faults created positive relief structures such as the Central Basin Platform and the Ozona Arch, which split the Tobosa Basin into its constituent sub-basins (Frenzel et al., 1988; Shumaker, 1992).

The Laramide Orogeny occurred after an extended period of passive tectonism towards the end of the Mesozoic (Frenzel et a., 1988). After the Permian, tectonism did not alter the structure of the Midland Basin significantly, but deformational processes did result in uplift that would expose Paleozoic strata to the west above sea level. The

intervals of "Volcanic" and "Basin and Range" deformation during the Cenozoic would supply additional heat flow to the southwestern portion of the GPB region (Horak, 1985; Atchley et al., 1999). Faulting associated with the Laramide Orogeny exposed GPB strata at the surface in the Guadalupe and Sacramento Mountains (Horak, 1985; Atchley et al., 1999).

2.2 Depositional History

Strata within the Tobosa Basin consist primarily of fine-grained sandstones and carbonates. Deposition began in the Late Cambrian with the Hickory Sandstone Member (Frenzel et al., 1988). Stratal accumulation was discontinuous over the next ~160 Ma (Galley, 1958; Frenzel et al., 1988). By the Late Devonian, the Tobosa Basin was no longer tectonically active. This period is marked by the deposition of the Woodford black shale, an important petroleum source rock in the region (Frenzel et al., 1988). The Tobosa Basin was completely filled and no longer existed as a separate depositional basin by the Mississippian.

The Precambrian geology of the Tobosa Basin is poorly constrained, due to a lack of both drilling and geophysical data. Many drill cores have reached the Proterozoic rocks, but have only penetrated a few meters. The little data available suggest that the Precambrian rocks consist of igneous, volcanic, and metasedimentary rocks (Frenzel et al., 1988). One deep drill hole on the Central Basin Platform penetrated through 4,400 m of layered gabbro underneath Permian sedimentary rocks (Keller et al., 1989). Few age constraints for these Proterozoic rocks are available, but the data suggest that there was an orogenic event approximately 1.0 to 1.3 Ga, due to arc-continent and continent-

continent collision along the southern margin of Laurentia (Mosher, 1998). This collision resulted in the emplacement of a mafic layered intrusion underneath the Central Basin Platform (Mosher, 1998).

As a result of post-Grenville uplift and exhumation, the depocenter for the Tobosa Basin was potentially above sea level until the deposition of the Late Cambrian Hickory Sandstone Member of the Riley Formation. This hiatus in deposition is reflected by the complete absence of Early and Middle Cambrian strata within the Permian Basin region. Late Cambrian strata include sandy, glauconitic limestones that underlie the Lower Ordovician Ellenburger Group. The dominant lithology of the Ellenburger Group is calcitic limestones, with some dolomitic members. During the Middle Ordovician, the Simpson Group was deposited on top of the Ellenburger Group. The Simpson Group consists of interlayered limestones, sandstones, and dark green shales. Overlying the Simpson Group is the Late Ordovician Montoya Formation. This formation is composed of fine, crystalline calcitic and dolomitic limestones. Siluran-Devonian strata are coarsely crystalline limestones interbedded with green shales and occasional anhydrite beds. Capping the Silurian-Devonian lithologies is the Late Devonian Woodford Shale, an organic rich, highly fossiliferous black shale. With the deposition of Early Mississippian strata and the burial of the Woodford Shale, the Tobosa Basin was filled and ceased to exist as a depocenter.

The Mississippian marked a new period of tectonic activity for the Permian Basin. Tectonic activity within the Permian Basin shifted from a relatively stable configuration to uplifted platforms and arches. By the Late Mississippian-Early Pennsylvanian, the Permian Basin was differentiated into the Midland and Delaware Basins by the Matador

Uplift to the north, the Diablo Uplift to the east, and the Central Basin Uplift along the mid-basin axis. Pennsylvanian strata within the Midland Basin are dominated by black-to-gray mudrocks in the basin center, with beds of carbonates and silts more common along the margins. Strata along the eastern and western boundaries of the basin are less than 300 m thick, thinning to less than 200 m towards the center (Hamlin and Baumgardner, 2012). During the Pennsylvanian period, the Midland Basin was tectonically stable, with the Mississippian-Pennsylvanian contact dipping slightly to the west. The depth to the base of the Pennsylvanian is roughly 3,000-3,500 m below the surface (Frenzel et al., 1988). In the northern part of the Midland Basin is the Horseshoe Atoll, a semicircular carbonate bioherm that contains significant oil accumulations within Pennsylvanian-age reservoirs (Frenzel et al., 1988). The atoll is composed of Strawn, Canyon, Cisco, and Wolfcamp carbonates and associated talus, ~309-284 Ma in age (Figure 2.3; Waite and Reed, 2014).

The Dean Sandstone was deposited during the Leonardian, roughly equivalent to the Kungurian epoch (279.3-272.3 Ma). This is the lowermost Leonardian formation in the Midland Basin, and it consists of fine grained siltstones and sandstones. The Dean Sandstone is overlain by the Spraberry Formation, which consists of gray shales and limestones interbedded with sandstones and siltstones. These two formations form the Spraberry Trend oil field, a highly productive play that has produced over 585 million barrels of oil (Frenzel et al., 1988). The evaporites of the overlying Salado Formation constitute the seal for the hydrocarbon systems of the Midland Basin. These salts were deposited during the Ochoan Period, and by the Late Ochoan the entire Permian Basin became a large evaporite basin.

2.3 Paleoenvironment and Paleoceanography

Based on fusulinid biostratigraphy and correlations to shelf strata, the basinal WC-D was deposited in the Late Pennsylvanian during icehouse climate conditions known as the Late Paleozoic Ice Age (LPIA), which lasted ~70 million years (Soreghan, 1994; Cleal and Thomas, 2008; Montañez and Poulson, 2013). Montañez and Poulsen (2013) reviewed the various environmental proxies that have been used to trace glaciation through time (Figure 2.2). The causes of this ice age are not well known, but climatic forcing took place over timescales equivalent to tectonic change (10^6-10^7 yrs) (Tabor and Poulsen, 2008). Initially thought to be a single, global glaciation event, evidence now suggests that the LPIA is actually a series of discrete glacial and interglacial periods. Recently, the presence of periglacial and glacial sediments have been recognized within the stratigraphic record in depocenters across Gondwana (Fielding et al., 2008a, 2008b; Isbell et al., 2012). The effects of glacial eustatic sea level change on coastal and shallow marine environments have been studied extensively, and repetitive, cyclic vertical facies patterns (cyclothems) are a common depositional motif in many localities (Boardman and Heckel, 1989; Rasbury et al., 1998; Saller et al., 1999a; Heckel, 2008; Greb et al., 2009; Eros et al., 2012; Belt et al., 2015).

The WC-D is believed to have been deposited during the Desmoinesian, Missourian, and Virgilian (North American) stages, concomitant with the high-frequency, high-amplitude eustatic sea level change associated with the LPIA (Figure 2.3) (Ross and Ross, 1987; Rygel et al., 2008; Eros et al., 2012; Montanez and Poulsen, 2013; Waite et al., 2014). Absolute dating of individual glacial-interglacial cycles during this time period has been impeded due to the uncertainty of the impact of local ice sheets, the diachronous

nature of glaciation, and finally the problem of dating multiple lithologies from the Late Paleozoic (Tabor and Poulsen, 2008; Isbell et al., 2012). During the LPIA, the Central Basin Platform (CBP) was subaerially exposed multiple times during sea level lowstands. Approximately 87 cycles were identified by Saller et al. (1994, 1999a, 1999b) on the CBP, most of which are bounded by exposure surfaces. These cycles are equivalent to the Strawn, Cisco, Canyon, and Wolfcamp Formations. Radiometic (U-Pb) age dates calculated from pedogenic carbonates suggest that cycle lengths are 143 ± 64 ka, mirroring the Milankovitch-style eccentricity cycles of the Pleistocene (Rasbury et al., 1998).

The Late Pennsylvanian-Early Permian was a period of dynamic climate change due to the formation of the Pangaean supercontinent, which significantly impacted atmospheric circulation patterns (Tabor and Poulsen, 2008; Horton et al., 2012; Heavens et al., 2015). Tabor and Poulsen (2008) used climate-sensitive lithologic proxies plotted on paleo-reconstruction maps to determine the changes in the position of the Inter-tropical Convergence Zone (ITCZ) through the interglacial and glacial intervals. During glacial events, the ITCZ contracts in width, resulting in the subtropical and arid belts migrating towards the equator (Soreghan, 1994; Tabor and Poulsen, 2008). The exact latitudinal location of the Midland Basin during this time period is not well constrained, but it believed to have been positioned at approximately 0-10° N (Algeo and Heckel, 2008; Blakey, 2011). At this latitude, the climate of the Midland Basin during glacial periods is believed to have been relatively cool (Tabor and Poulsen, 2008; Montanez and Poulsen, 2013; Heavens et al., 2015). In addition, the position of the Midland Basin may have experienced a monsoonal climate, due to differential heating of the Panthalassic

Ocean and Pangaea, potentially impacting sedimentation by affecting wind directions and rates of runoff from the continent, as well as driving winds that affected water column stratification and stability (Algeo and Heckel, 2008; Montanez and Poulsen, 2013).

Precipitation into the Midland Basin was most likely controlled by a weak or discontinuous monsoon pattern, and not strongly impacted by high-altitude, alpine glaciers (Heavens et al., 2015). Alpine glaciation of the Ancestral Rocky Mountains has been documented for the Early Permian, but it is lacking highly precise age control (Soreghan, 2014). The Late Pennsylvanian is characterized as a relatively temperate interval, after which glaciation reached the maximum extent during the Late Paleozoic. Therefore, it is unlikely that high-altitude glaciation was a key factor in the precipitation budget for the Midland Basin during the deposition of the WC-D (Montanez and Poulsen, 2013; Soreghan, 2014; Heavens, 2015). Instead, since deposition occurred during a more temperate interval, the amplitude of sea level variability is believed to have been a more significant control. This results in more moisture availability and stronger monsoons due to the surface area of available water increasing during sea level highstands (Heavens, et al., 2015).

It is probable that the precipitation of the Midland Basin was seasonal, as a result of the monsoonal climate and proximity to the equator (Figure 2.4; Blakey, 2011). Large seasonal swings in the amount of precipitation are anticipated to cause erosion of sediment from high relief areas into the basin or other storage areas along the transport network. The Late Pennsylvanian Midcontinent Sea (LPMS) was an epeiric sea that spanned the North American midcontintent and was connected to the Panthalassic Ocean via the Greater Permian Basin Seaway. Variations in the sea level of the LPMS resulted

in the deposition of cyclothems across the U.S. Midwest (Algeo and Heckel, 2008). Continental runoff into the LPMS resulted in a surface layer of water with reduced salinity, albeit close to normal marine salinity due to good mixing with open ocean waters (Algeo and Heckel, 2008). This contributed to the establishment of a strong pycnocline within the Midland Basin, driven by both the temperature and salinity differences between terrestrial run-off and the pre-conditioned bottom waters of the Panthalassic Ocean (Algeo et al., 2008; Algeo and Heckel, 2008). The bottom waters were pre-conditioned in such a way that they were denitrified and oxygen poor, due to primary productivity occurring in equatorial Panthalassa (Algeo et al., 2008; Algeo and Heckel, 2008). Pervasive benthic anoxia of the LPMS is demonstrated by widespread deposition of black shales on the Kansas shelf during sea level highstands (Algeo and Heckel, 2008). A type of pseudo-estuarine circulation was established with freshwater inputs on the eastern end of the LPMS and saline open ocean water on the west end. Waters of the LPMS were recharged via a circuitous path that passed through the GPB and connected with the Panthalassic Ocean (Algeo et al., 2008; Algeo and Heckel, 2008).

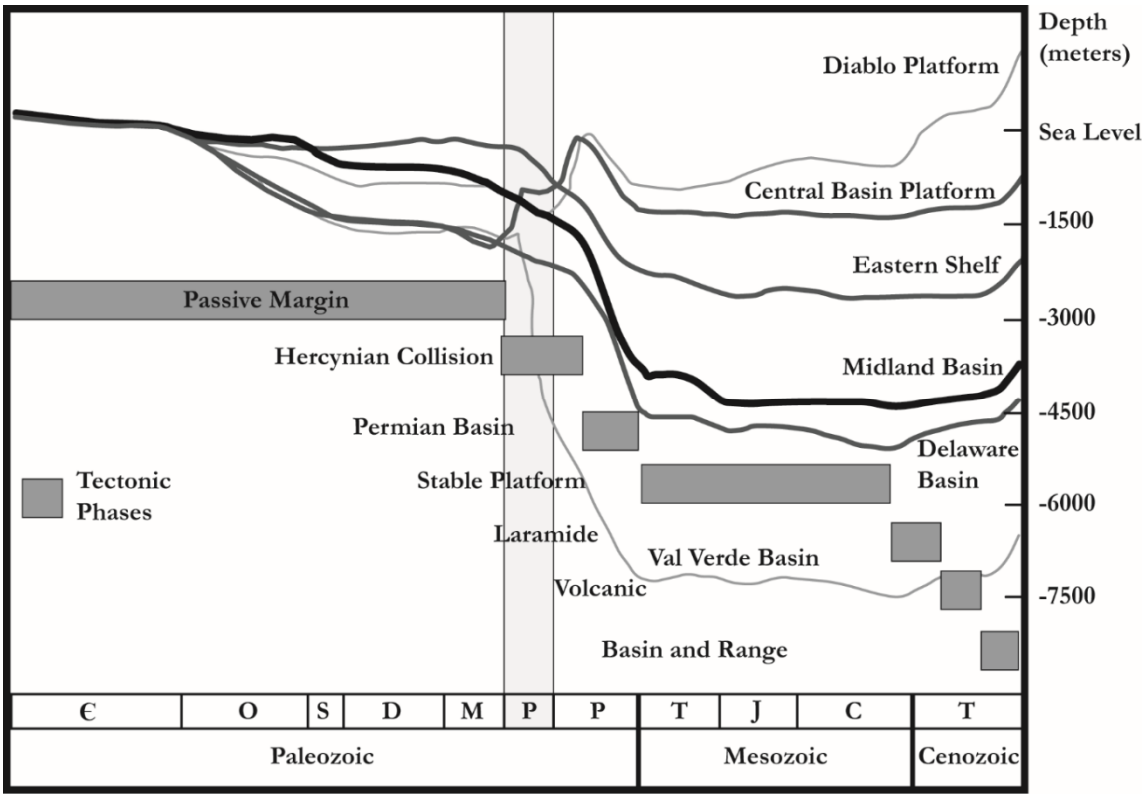

Figure 2.1. Tectonic History of the Greater Permian Basin
The subsidence profiles delineate the top of the Precambrian basement relative to modern day sea level for features of the GPB. The Midland Basin is represented by the thick black line. The CBP, Eastern Shelf, and Delaware Basin are the dark grey lines. Timing of tectonic phases are shown by the gray rectangles. The Pennsylvanian is shown in the light gray rectangle, concurrent with the Hercynian Collision. (Horak, 1985; Ryan, 2016).

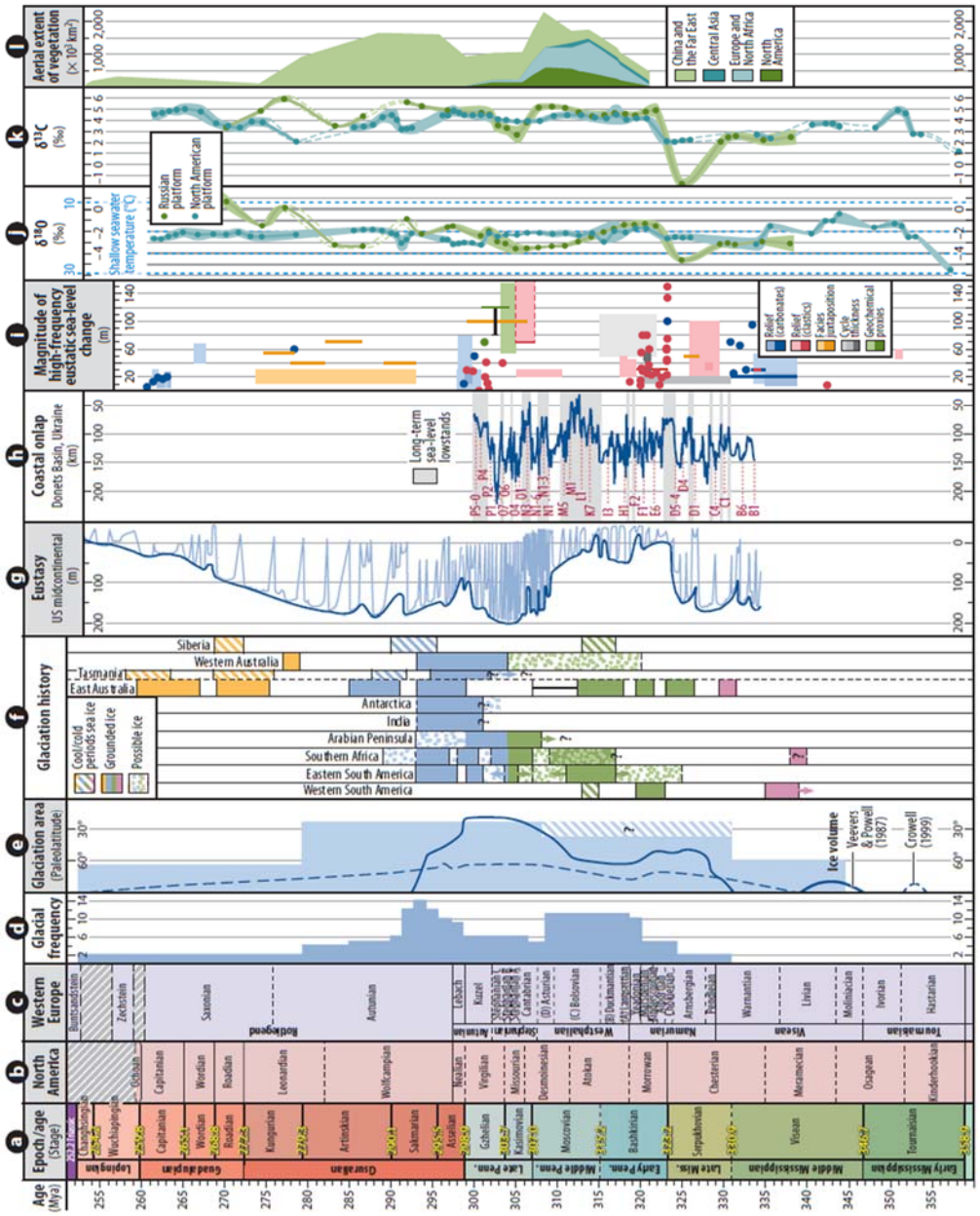

Figure 2.2: Summary of Late Paleozoic Ice Age conditions.
This figure summarizes multiple review papers centered on describing the climate conditions of the Mississippian to the Pennsylvanian, inferred from geological proxies. The present study is concerned with the Desmoinesian to Virgilian North American stages (~299-309 Ma). This period is characterized by short, high-frequency interglacial-glacial cycles superimposed over a longer warming trend. The icehouse conditions persisted through the Pennsylvanian and into the Early Permian, until the climate shifted to a long, global greenhouse period (from Montanez and Poulsen, 2013).

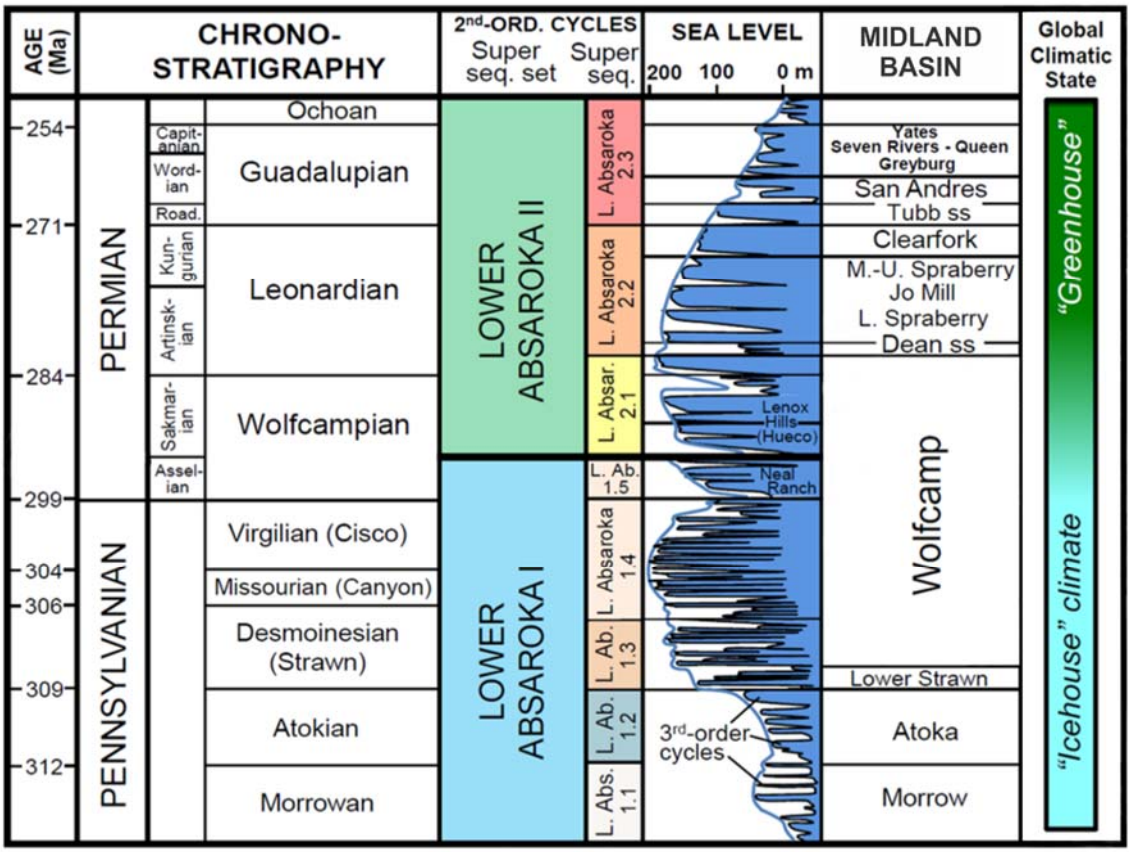

Figure 2.3: Stratigraphy of the Midland Basin (modified from Waite and Reed, 2014). The chronostratigraphy, sequences, and eustatic sea level curve for the Midland Basin were produced in prior research (Sloss, 1969; Ross and Ross, 1987). The interval of interest includes the Lower Absaroka 1.3 to 1.4, contemporaneous to the Desmoinesian through the Virgilian stages. The Strawn, Canyon, and Cisco Formations are the time-equivalent strata of the Wolfcamp-D, found on the Central Basin Platform and Eastern Shelf.

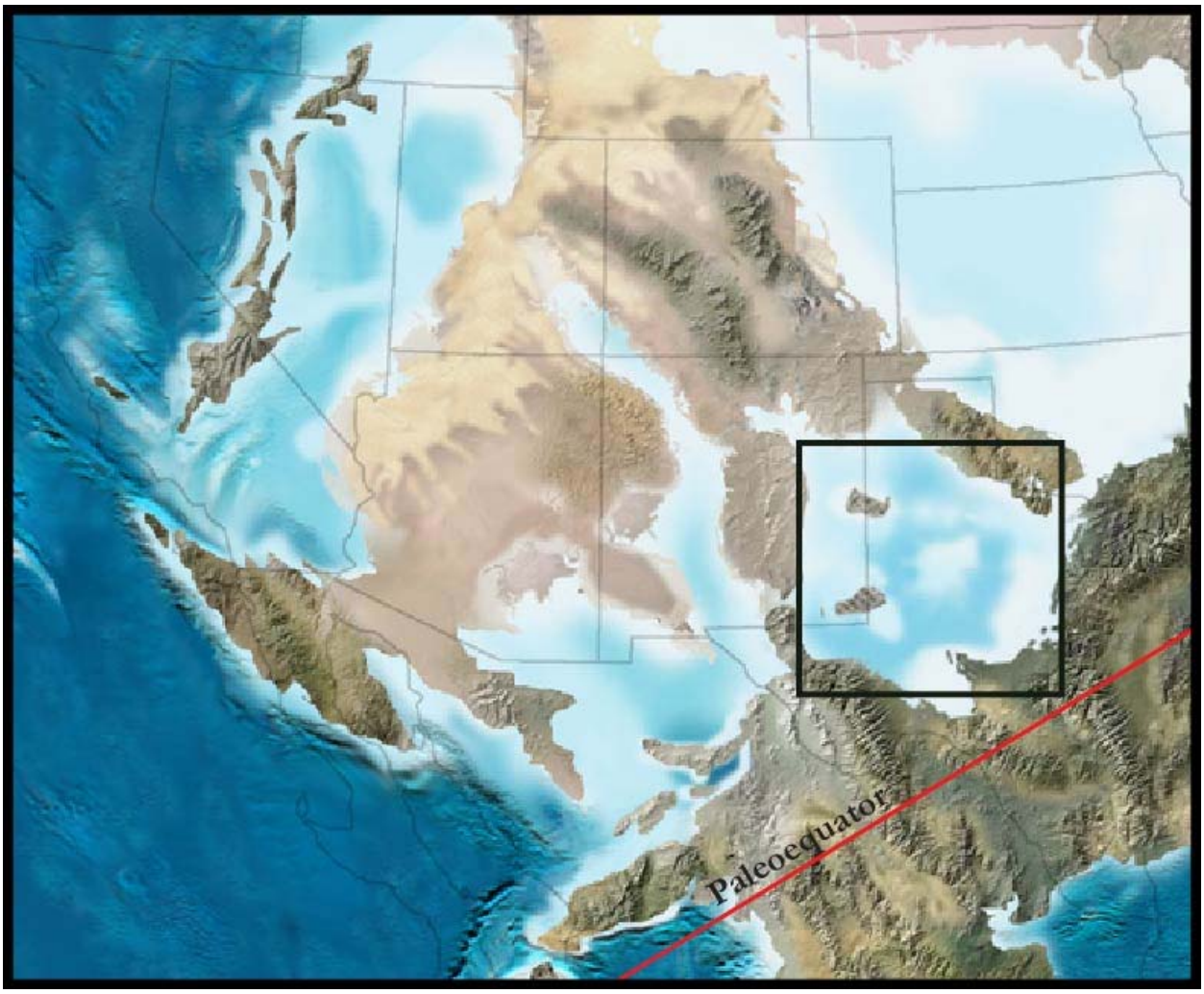

Figure 2.4. Paleogeographic reconstruction of the southwest and midcontinent of North America from the Late Pennsylvanian, approximately 300 Ma ago (modified from Blakey, 2013). The black rectangle shows the location of the Greater Permian Basin, with the Midland Basin situated on the eastern side. The Midland Basin is interconnected with the Panthalassic Ocean to the west and the Late Pennsylvanian Midcontinent Sea to the north and east. Figure 1.1 shows a more detailed description of geologic structures within the Midland Basin.

CHAPTER THREE: METHODS

An integrated approach was taken to characterize and describe subsurface drill core for this study, combining both chemostratigraphic and lithostratigraphic analyses. Pioneer Natural Resources donated the two-thirds working section of a four-inch diameter core from Martin County, which measured approximately ~388 ft long and consisted of alternating layers of mudrocks and carbonates. The cored interval extends from the top of the Strawn Formation, through the WC-D, and into the WC-2. The location from which the core was collected is the northern part of the Midland Basin, approximately 20 km down dip from the Horseshoe Atoll. The core was received in good condition; most intervals were intact, while only a few minor spots were marked by heavy fragmentation. Some sections of core that were reduced to rubble may have been impacted by the recovery process itself, due to the contrasting hardness between clayey mudrocks and dense carbonates. Decompression fractures are prevalent throughout the core, reducing the quality in some sections (Figure 3.1). Some sections (approximately 7%) were missing due to sub-sampling by Pioneer Natural Resources prior to delivery. The amount of missing section was determined by comparing the number of missing X-ray fluorescence (XRF) points and dividing that by the expected number of points for a whole core, 2168 points compared to a theoretical 2331 points if the core were continuous.

Lithostratigraphic description of the core followed the methodology described by Campbell (1967), Bohacs (1990), and Bohacs et al. (2014). Characterization of grain size, mineralogy, texture, sedimentary structures, bedding, fossil content, and color was used to provide information on the environment of deposition and sedimentary processes.

Lithology (especially carbonate content) was inferred by the reaction of the core to dilute hydrochloric acid. Carbonates were classified using Dunham's scheme when appropriate (Dunham, 1962; Flügel, 2004). Hand sample observations were complemented with a petrographic thin section report produced by CoreLab, provided to the project by Pioneer Natural Resources (Pioneer Natural Resources 2013, personal communication). The lithostratigraphic observations were tabulated in a MS Excel® table, and sequentially moved to a master, Adobe Illustrator® file to produce a composite lithologic log.

Two-inch intervals were marked on the face of the core for chemical analysis via a handheld, energy dispersive XRF gun (Bruker Tracer IV-SD™), following a modified procedure developed after Rowe et al. (2012) (Figure 3.2). Orange stickers were used to mark the intervals for scanning, and prior to each analysis, the sample was washed in distilled water and dried with compressed air. The XRF gun is fitted with a 40 keV and 60 μA x-ray tube. Chemical data were collected over 90 seconds in order to maximize the signal-to-noise ratio. Marked sample points were analyzed twice, once each for major and trace element chemistry, respectively. Major elements, with atomic number 11-26, were collected at 15 keV and 35 μA under vacuum conditions of 9 torr. Trace elements, with atomic number 20-51, were collected at 40 keV and 15 μA without a vacuum. The rock chosen as a reference material was SARM-41, a shale standard from South Africa (Ring, 1993). SARM-41 was run at the beginning and end of each three-foot core box, in order to determine stability and reproducibility of the ED-XRF. Raw counts collected by the gun were calibrated and converted to elemental weight percentages using Bruker proprietary software and the empirical calibrations of Rowe et al. (2012). The detection limits of the major and trace elements are listed in Tables 1 and 2, respectively. The

calibrations of Rowe et al. (2012) were determined by comparing results of various analytical measurements (e.g., ICP-MS and WD-XRF) to the compositions of a suite of 90 mudrocks. Accuracy of the measurements decreases for lighter elements, such as sodium and magnesium. This is an important consideration, due to the significance of Mg in the formation of some carbonate lithologies. The geochemical cutoffs used for differentiating facies types are an interpretive guide used in conjunction with the lithostratigraphy, following the approach outlined by Baldwin (2016) and Ryan (2016).

Organic geochemistry datasets (organic carbon) were provided by Pioneer Natural Resources to supplement our analysis. Additional subsampling and analyses was conducted at the University of Kentucky in order to augment the dataset. Pioneer Natural Resources delivered LECO-derived total organic carbon (TOC) values. An additional 36 samples were crushed, powered, sieved, and shipped to the University of Utah Stable Isotope Ratio Facility for Environmental Research (SIRFER). Elemental and isotopic data was obtained by leaching powered samples with hydrochloric acid, until the mixture contained no carbonate. The slurry was then washed using distilled water (Connin et al., 1997). Analysis was performed using an elemental analyzer coupled to an isotope ratio mass spectrometer calibrated for carbon and nitrogen (EA-IRMS-CN). Stable isotope ratios for carbon ($\delta^{13}C_{ORG}$ ‰) and nitrogen ($\delta^{15}N_{ORG}$ ‰), TOC, total nitrogen, and carbon to nitrogen ratios (C:N) were provided by the analysis. Stable isotope data are presented using the standard delta (δ) notation, which represents the difference between the sample and internationally accepted standard, in per-mille (‰) units. This is calculated using the formula:

$$\delta_{(\mathrm{sa})} = \frac{R_{(sa)} - R_{(st)}}{R_{(st)}} \times 1000$$

Where $R_{(sa)}$ is the sample isotopic ratio ($^{13}C/^{12}C$ or $^{15}N/^{14}N$), and $R_{(st)}$ is the isotopic ratio of the appropriate standard, the Vienna Pee Dee Belemnite (VPDB) and atmospheric air (AIR) for carbon and nitrogen, respectively (Bowen, 1991).

Abundance and variation of maceral types within the black mudrocks of the Martin County core were determined via petrographic point counts. Organic petrography was used in order to help determine the source of organic matter in the samples. Subsamples (n=19) for maceral analysis were crushed and sieved to 850 μm (Ting, 1978). The coarse fraction was mixed into epoxy and allowed to settle and dry in ring molds. After the epoxy set, the pucks were cut, polished, and oiled. Point counting was conducted under white and fluorescent light using a reflected light microscope at the Kentucky Geological Survey (Ting, 1978; Chapman et al., 2015).

An absolute age for the black mudrocks within the core was calculated using the rhenium-osmium (Re/Os) geochronometer, based on the decay of rhenium-187, which yields osmium-187. Rhenium naturally occurs as two isotopes, ^{185}Re (37.4% atomic) and ^{187}Re (62.6% atomic) (Shirey and Walker, 1998). Rhenium-187 undergoes beta decay by the emission of an election, resulting in osmium-187. The decay constant of 1.666×10^{-11} for ^{187}Re-^{187}Os has been calculated using high resolution isochrons generated from iron meteorites (Shirey and Walker, 1998 and references therein). Both Re and Os are known to be incorporated into black mudrocks either by redox reactions at the sediment-water interface, or into the organic fraction (Kendall et al., 2004). The ratio of $^{187}Os/^{188}Os$, a measure of the Os composition of seawater, is composed of radiogenic Os derived from

continental weathering and unradiogenic Os produced from hydrothermal alteration of oceanic crust (Cohen et al., 1999). Therefore, measurements of Os can actually record changes in ocean chemistry on timescales shorter than those records by Sr, because the residence time for Os is ~40 ka (Cohen et al., 1999). Mudrocks with both high TOC and sulfide content were selected for Re-Os measurements, as these samples were most likely to have measureable Re and Os abundances. Samples were collected from the three cores delivered by Pioneer Natural Resources (Martin County, Midland County, and Upton County cores; Baldwin, 2016; Ryan, 2016) at depths believed to be coeval.

The Re-Os analysis took place in the TIMS laboratory at Miami University of Ohio using the following procedure. Spikes of known rhenium and osmium isotopic composition were added to a 15 mL jar. The black mudrock sample was ground to a fine powder in a ceramic disc mill in order to avoid metal contamination, weighed out to 0.1 g, and added to a Carius tube (CT). The CT was placed in an ethanol-water ice bath. A mixture of hydrochloric and nitric acid, with a molar ratio of 1:3, was added to the CT in the ice bath. The CT was then sealed with a blow torch, allowed to warm up to room temperature, and then placed in an oven at 240 °C for at least 72 hrs. After 72 hrs had passed, the mixture in the CT was poured into a 15 mL beaker on a hot plate set to 115 °C for osmium distillation. The beaker was connected via tubing to a 30 mL beaker containing HBr, in a water ice bath (Figure 3.3). The gas flow was adjusted such that the bubbling rate was approximately 1-2 bubbles per second. This distillation process separates the osmium from the rhenium. After 2.5 hrs, the tubing was disassembled and the residues containing both the rhenium and osmium were dried down at 90 °C. Osmium was then further concentrated via microdistillation and evaporated down to 1-2 μL.

Rhenium was separated from the rest of the sample via an anion exchange column using AG1-8X resin, and then dried down. Once both the osmium and rhenium were dried, samples were loaded into a Thermo Finnigan Triton™ negative-ion TIMS (thermal ionization mass spectrometry) for analysis of isotopic ratios and concentrations. The osmium can be analyzed on a standard rhenium filament, but the rhenium must be sampled using a platinum filament to prevent interference. Osmium isotopic ratios were corrected for mass fractionation using the ratio $^{192}Os/^{188}Os = 3.0826$. Oxygen isotope corrections for rhenium and osmium used the values of Neir (1950). The age was calculated with Isoplot ver. 4.15, a Microsoft Excel™ add-in, using the Model 1 fit for the regression (Ludwig, 2003).

Mudrock Major Calibration (MA1.cfz)				
Element	**Symbol**	**Atomic No.**	**Minimum**	**Maximum**
Sodium	Na	11	964 ppm	8606 ppm
Magnesium	Mg	12	2412 ppm	10.25%
Aluminum	Al	13	9103 ppm	13.07%
Silica	Si	14	3.75%	38.20%
Phosphorous	P	15	87 ppm	9819 ppm
Sulfur	S	16	200 ppm	5.35%
Potassium	K	19	1411 ppm	4.30%
Calcium	Ca	20	786 ppm	34.66%
Titanium	Ti	22	479 ppm	5336 ppm
Vanadium	V	23	22 ppm	1720 ppm
Chrome	Cr	24	10 ppm	295 ppm
Manganese	Mn	25	77 ppm	1239 ppm
Iron	Fe	26	4267 ppm	6.53%
Cobalt	Co	27	1.4 ppm	46.8 ppm
Nickel	Ni	28	14 ppm	302 ppm
Copper	Cu	29	5 ppm	429 ppm
Zinc	Zn	30	20 ppm	836 ppm
Barium	Ba	56	30 ppm	1.50%

Table 3.1 Major Element Calibration Limits

Mudrock Trace calibration (TR2.cfz)				
Element	**Symbol**	**Atomic No.**	**Minimum**	**Maximum**
Calcium	Ca	20	786 ppm	34.66%
Titanium	Ti	22	479 ppm	5336 ppm
Chrome	Cr	24	10 ppm	295 ppm
Manganese	Mn	25	77 ppm	1239 ppm
Iron	Fe	26	4267 ppm	6.53%
Cobalt	Co	27	1.4 ppm	46.8 ppm
Nickel	Ni	28	14 ppm	302 ppm
Copper	Cu	29	5 ppm	429 ppm
Zinc	Zn	30	20 ppm	836 ppm
Arsenic	As	33	<1 ppm	69 ppm
Rubidium	Rb	37	6 ppm	224 ppm
Strontium	Sr	38	39 ppm	869 ppm
Yttrium	Y	39	6 ppm	62 ppm
Zirconium	Zr	40	17 ppm	338 ppm
Niobium	Nb	41	2 ppm	16 ppm
Molybdenum	Mo	42	<1 ppm	166 ppm
Tin	Sn	50	<1 ppm	14 ppm
Antimony	Sb	51	<1 ppm	47.1 ppm
Barium	Ba	56	30 ppm	1.50%
Lead	Pb	82	<1 ppm	28 ppm
Thorium	Th	90	2 ppm	14 ppm
Uranium	U	92	1 ppm	51 ppm

Table 3.2 Trace Element Calibration Limits

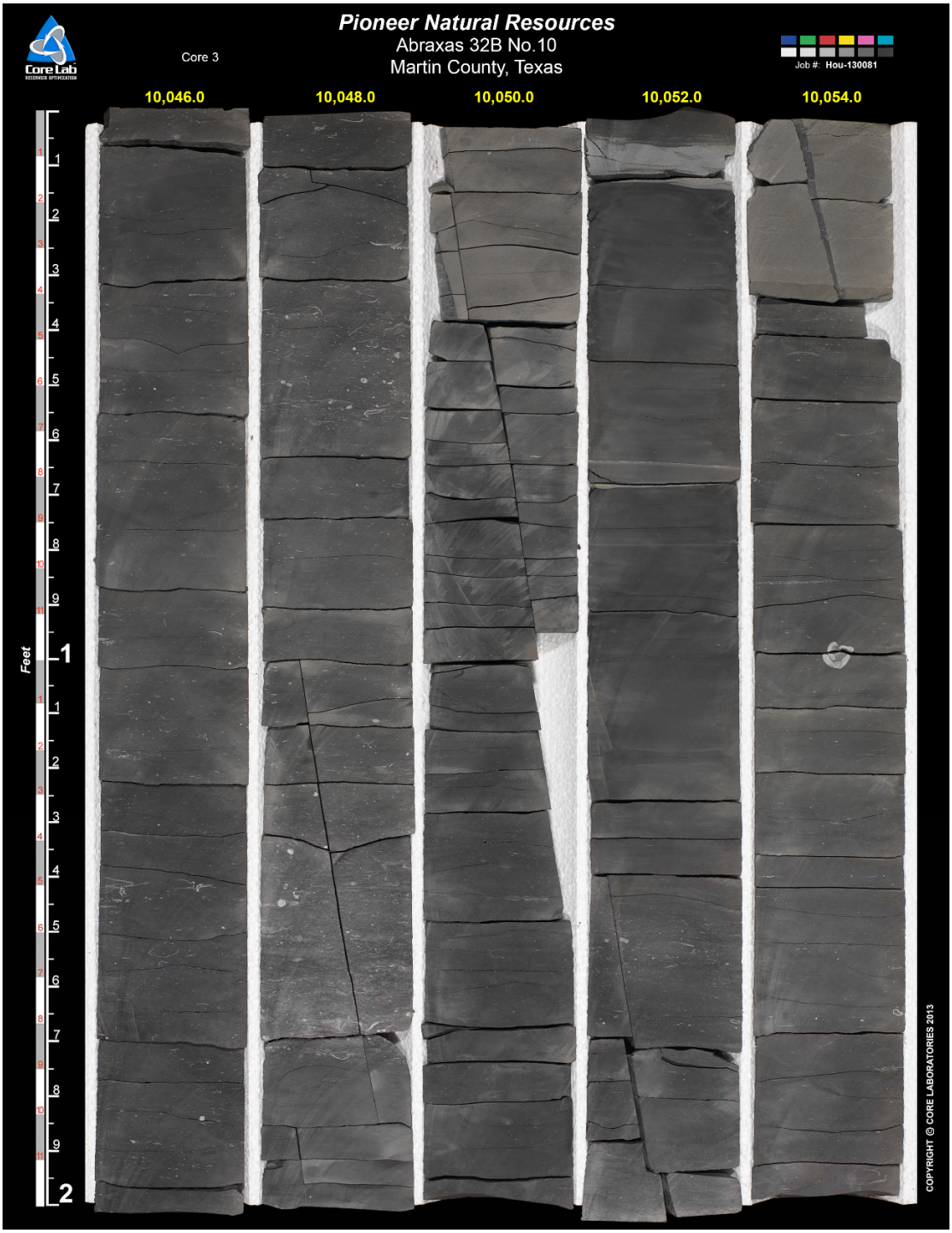

Figure 3.1: High-resolution photo of the one-thirds archived section of Martin County core.

Vertical decompression fractures of the core can be observed; these formed as the core was extracted from depth. Horizontal fracturing ("poker chips" or "biscuiting") may be characteristic of the rocks at reservoir depths (Sarkar, 2017 personal communication) Intervals of missing core are indicated with foam spacers (not shown).

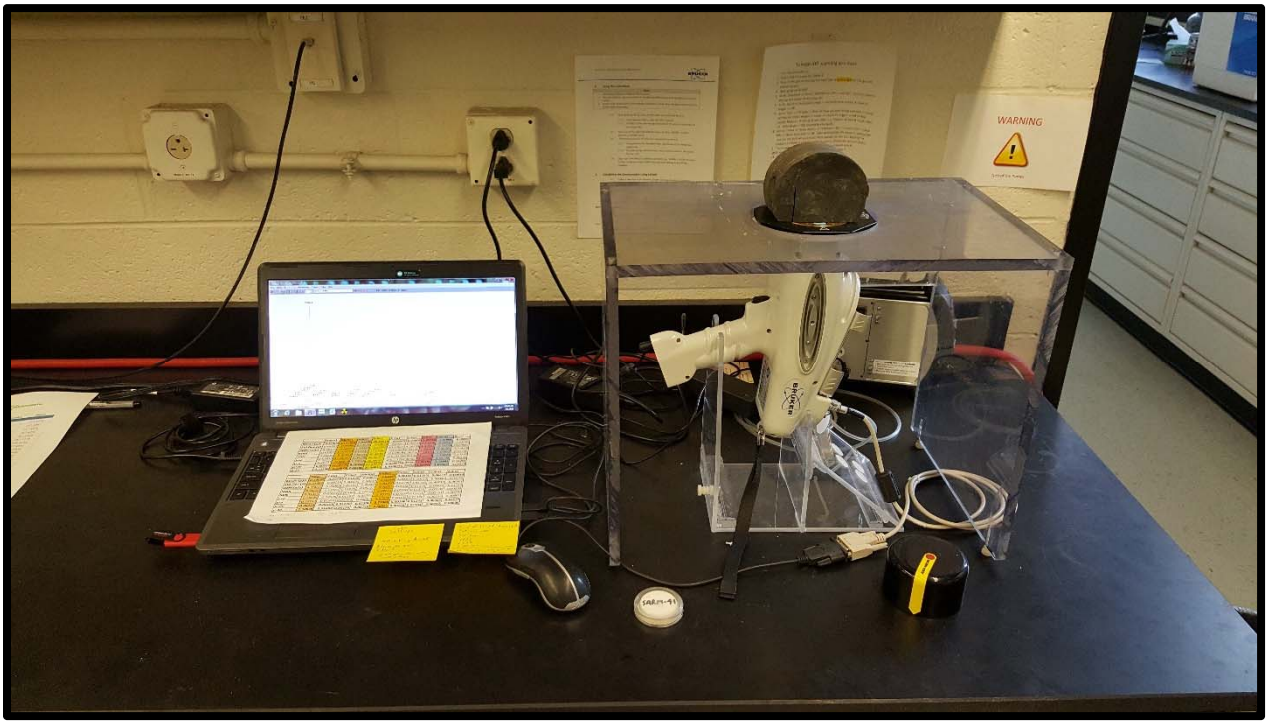

Figure 3.2: Energy Dispersive X-ray Fluorescence.
Energy dispersive X-ray fluorescence (ED-XRF) setup for the elemental analysis of the two-thirds working section of the core. The Plexiglas® shield was used to support heavier sections of core as protection for the device. The white puck is the SARM-41 standard used to calibrate the instrument.

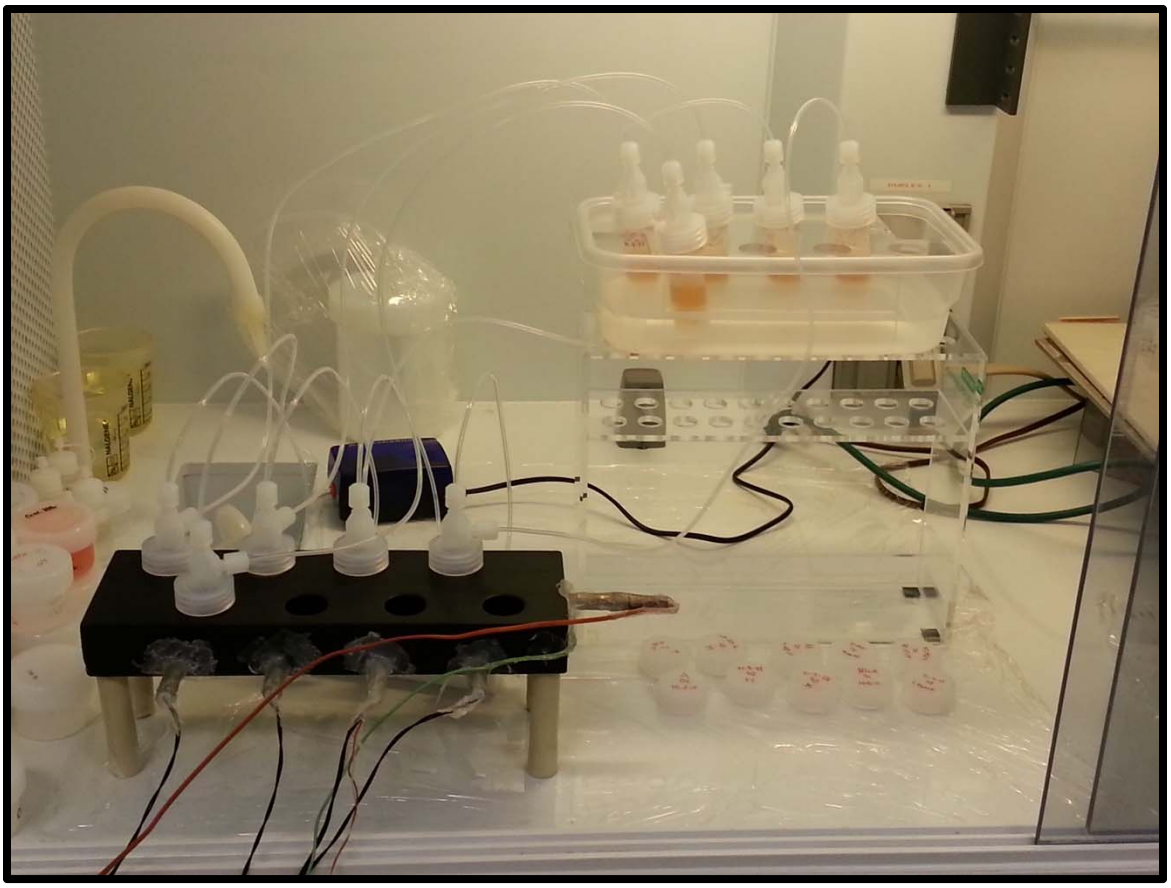

Figure 3.3. Distillation and Separation of rhenium/osmium from samples
The sample and aqua regia (nitric and hydrochloric acid) mixture is placed into a hot block (left). Tubing is connected to plastic beakers placed into an ice bath. The osmium travels through the tubing and is condensed in the beakers on the right while the rhenium stays in the beakers on the left.

CHAPTER FOUR: RESULTS

4.1 Lithofacies Results

Nine different lithofacies were identified in the WC-D and WC-C2 intervals of the Martin County core; these facies consist of a variety of siliciclastics and carbonates. The frequency and distribution of facies types changes vertically through the stratigraphic section (Figure 4.1). The facies present include three types of siliciclastic mudrocks, four types of carbonates, one minor heterolithic facies, and one diagenetic type. The three siliciclastic facies include two variations of black mudrock (BMR-1 and BMR-2) and a gray mudrock (GMR). Carbonate facies are represented by a collection of wackestones, packstones, grainstones, and dolostones (WKST, PKST, GRST, and DOL, respectively). Lastly, there are heterolithic beds of siliciclastic and carbonate lithologies (MIXED). The most prevalent facies within the WC-D interval is the GMR. Percent abundances for the WC-C2 were calculated, and BMR-2 facies dominates, but it remains unclear if this is truly representative of the full WC-C2 section.

Two types of black mudrock can be distinguished within the Martin County core, Black Mudrock 1 (BMR-1) and Black Mudrock 2 (BMR-2). The bedding of BMR-1 and BMR-2 is typically massive, with occasional continuous to discontinuous sub-parallel laminations of silt (either siliceous or calcareous), and clay. In hand sample, the color of both black mudrocks is dark gray to black. An important sedimentological characteristic that is diagnostic of BMR-1 are large, dense nodules absent of internal structure, which at times disrupted bedding. While frequently indistinguishable macroscopically, the two facies are geochemically distinct. XRF analysis revealed that BMR-1 is characterized by low relative amounts of aluminum (<6%) and high percentages of silicon (>26%). Total

organic carbon (TOC) in BMR-1 ranges from 1.19% to 7.66%, with an average value of 4.17%. Trace metal abundances (e.g., molybdenum and chromium) are relatively high in BMR-1 (Supplemental Table 1). Analysis via XRF revealed that the nodules in BMR-1 are composed of either pyrite or phosphatic minerals. Pyrite occurs as disseminated crystals, framboids, or replacing organic matter. The variability in pyrite morphologies found within BMR-1 rocks implies that pyrite formed early during diagenesis (Scott and Lyons, 2012). Framboidal pyrite tends to form first, with the smaller, euhedral crystals developing secondarily (Scott and Lyons, 2012). Body fossil content of BMR-1 facies is very low to absent. In thin section, BMR-1 fabrics occasionally show a preferred orientation of particles (Figure 4.2). The elongate, white particles are compacted algal cysts (*Tasmanites)* that were filled with silica, most likely associated with the dissolution of sponge spicules and radiolarians during burial and subsequent heating (Schieber, 1996; Schieber et al., 2000). The prevalence of biogenic silica indicates that surface waters at the time of deposition were productive. This is consistent with high TOC and phosphate nodule content of BMR-1 rocks. Both the relatively high abundances of TOC and pyrite suggest that bottom water conditions during deposition were anoxic and potentially even euxinic (Scheiber, 1996; Bohacs, 1998; Scott and Lyons, 2012). The ratio of molybdenum to TOC is ~4.01 (Figure 4.3).

The BMR-1 facies type is interpreted to have been deposited by pelagic fallout in a basin marked by low rates of sediment accumulation that was potentially influenced by upwelling. The bottom water chemistry is inferred to be anoxic to euxinic due to the high TOC, pyrite content, and abundances of trace metals (Mo and Cr) of BMR-1 intervals. Processes that affect trace metals tend to operate more efficiently under anoxic and

euxinic conditions. Reduced valence states of trace metals are more easily bonded to organic complexes, precipitated as insoluble oxides, or incorporated in solid state solutions of sulfides (Algeo and Maynard, 2004). Low bottom water oxygen content allows for the preservation of organic matter that would otherwise be consumed by microbial respiration processes. The evidence for upwelling comes from the presence of the phosphate nodules and lenses, as well as the flattened *Tasmanites* cysts. Upwelling currents bring nutrient-rich bottom waters to the surface, increasing primary production in the photic zone (Algeo et al., 2008). Most beds of BMR-1 are massive, with laminations occurring infrequently. Fissile intervals are absent, resulting in this facies type being designated as a mudrock instead of a shale. Classic shales, such as the Ohio Shale from the Devonian, contain ubiquitous laminations and are highly fissile (Ettensohn et al., 1988; Potter et al., 2005). Even though the compressed *Tasmanites* casings align parallel to bedding planes, there is no indication that this affects the degree of fissility in BMR-1 beds. However, these silca filled cysts, which raise the overall %Si of BMR-1 to highest of the dataset, are very important to the brittleness and hardness of these rocks (O'Dell et al., in prep).

The second black mudrock facies, BMR-2, resembles BMR-1 in hand sample, but has a different geochemical signature. Like BMR-1, the fabric of BMR-2 is typically massive, with rare continuous to discontinuous sub-parallel laminations (Fig. 4.2). Fossils are more prevalent in BMR-2 compared to BMR-1 and occasionally show replacement of bioclasts with pyrite. Bioturbation, in the form of horizontal and vertical burrows, are present within BMR-2 and frequently exhibit pyritization. In thin section, BMR-2 shows disrupted fabrics due to these burrows, as well as compaction surrounding fossil

fragments. Phosphatic nodules are rare to absent in BMR-2. Pyrite is relatively common in the mineral matrix, either forming *in situ* or replacing organic matter. Most fossil fragments in thin section show evidence of complete replacement by silica or plagioclase (Pioneer Natural Resources, 2013 personal communication). Some fossils show no replacement, whereas others show silica replacement along the edge of the fossil. *Tasmanites* is present in BMR-2, but these cysts are dispersed in the matrix and do not form discrete laminations, as in BMR-1. The geochemical signature of BMR-2 is characterized by high relative aluminum content (>6%) and low silicon content (<26%) (Supplemental Table 1). Black mudrock 2 beds are markedly thicker than BMR-1 beds, with BMR-2 thicknesses ranging up to 5 ft. The TOC content of BMR-2 ranges from 0.47% to 4.99%, with an average of 1.81%.

We interpret BMR-2 to have been deposited by a similar mechanism as BMR-1, suspension fallout in a marine environment characterized by elevated primary productivity. However, we interpret several distinct environmental differences that help to explain the different chemistry of these black mudrock facies. Anoxia is interpreted to be less pervasive during deposition of BMR-2 intervals. Evidence for this lies in TOC and trace metal (Mo, Cr) content, which are significantly reduced in BMR-2 beds compared to BMR-1. Bioturbation is likely the cause of the discontinuous bedding fabric, and is an indication for the presence of benthic fauna (Hoffman et al., 1998). The existence of bioturbating fauna implies that oxygen was more available on the sea floor during the deposition of BMR-2. The preservation of organic matter is linked to oxygen content. As oxygen content increases, the rate of bacterial degradation and consumption of organic matter increases, thus decreasing the organic matter that is preserved. This is

reflected in the decrease in TOC seen in BMR-2 facies. Furthermore, the TOC content of BMR-2 is further diluted by an increase in clastic detritus, as shown by the increase in %Al content of BMR-2, relative to BMR-1. While productivity levels may not change, a decrease in the preservation potential and an increase in the dilution results in the lower average TOC content. These findings corroborate the findings of Ryan (2016) and Baldwin (2016) in two cores from the WC-D collected from Midland and Upton counties, respectively.

The third mudrock facies type is a gray mudrock (GMR). This facies type is characterized macroscopically by its gray color. The gray color is the result of an increase in the proportion of carbonate silt and sand. This is reflected in the inorganic geochemistry, which shows on average lower silicon, highrelative aluminum, and a significant increase in the calcium abundance compared to the BMR-1 and BMR-2 (Supplemental Table 1). The TOC of GMR is less than that of BMR-2, with an average value of 1.47% and discrete values ranging from 0.26% to 3.45%. Bedding is typically massive, with occasional laminations comprised of silt-sizedfossil fragments or siliciclastic detritus. Bioturbation and evidence of burrowing is prevalent throughout this facies, disrupting bedding fabrics in most instances; burrows are distinguishable based on sedimentological differences between the burrow wall and surrounding rock matrix (Figure 4.2). Scour marks are present and easily identified due to abundant fossiliferous material that is aligned to bedding planes directly above sharp basal contacts (Figure 4.2). Thin section analysis reveals that the matrix varies from siliciclastic clay and silt to lime mud. Fossiliferous debris is much more common compared to BMR-1 and BMR-2 facies, and it consists of whole intact fossils, skeletal fragments, or unidentifiable fossil hash.

Pyrite replacement of fossils is present, but less abundant compared to that found within BMR-2 facies.

Gray mudrock intervals are inferred to be deposited by a mixture of both suspension settling and weak turbidity flows. Normally graded beds of GMR vary in thickness from inches to over a foot thick. Gray mudrock beds also contain more fossiliferous material on average, occurring as both shell fragments and finer muds, which are probably derived from the Horseshoe Atoll and the Central Basin Platform. Elements that are indicative of terrestrial minerals (%Al, %K, and %Ti) are lower in GMR compared to BMR-1 and BMR-2. This is a result of the geographic location of the core location and its proximity to the Horseshoe Atoll, as flushing of shelf carbonates through turbidity currents would dilute the signature of material shed from continental rocks.

Carbonate lithofacies, WKST, PKST, GRST, and DOL, respectively, are represented within the Martin County core. The WKST and PKST beds tend to be thicker, on the foot scale, compared to GRST beds, which are on the order of one to five inches. The inorganic chemical composition of the carbonate facies is high in calcium (μ=29.14%) and low in both silicon and aluminum (μ=6.83% and μ=0.84%, respectively). Grainstone beds are bereft of identifiable fossiliferous material, but fine shell hash is abundant in this facies. Wackestone and PKST facies fossil assemblages include echinoderms, bivalves, ostracodes, gastropods, foraminifera, brachiopods, bryozoans, trilobites, ammonites, and algae. Both contain allochthonous material in the form of carbonate and siliciclastic intraclasts, which are on the order of 0.5-8 mm. Whole-fossil size is typically <1 mm, but can reach up to 750 mm; preservation was

variable but in some instances excellent, implying the potential for minimal post-mortem transport. The beds of PKST and WKST are massive, with neither preferred bedding fabrics nor scoured bases observable in hand specimens. Occasionally, reverse grading is present, with floating intraclasts of variable composition becoming larger towards the tops of beds (Figure 4.2). Intraclasts can be found within the PKST, typically composed of spiculitic mudstone, cemented algae, or other skeletal WKST or PKST with variable grain composition. Diagenetic alteration of carbonates is evident in thin section, with multiple examples throughout the core of silicification of fossil material, euhedral dolomite rhombohedra, and calcite infill of fossil void space (Figure 4.2).

Wackestone and PKST facies types are interpreted to be deposited during debris flows (Shanmugam and Benedict, 1987; Esposito and King, 1987; Benson, 1988). Within a single interval, PKST may gradually transition into WKST. These deposits are characterized by a lack of internal bedding and occasional reverse grading, both of which are traits common in these lithofacies types (Posamentier and Walker, 2006). Some of the interpreted WKST and PKST intervals do not feature reverse grading, but instead are relatively homogenous in grain size while lacking preferred organization. Projected clasts are present along basal layers of WKST and PKST, whereas erosional basal scour and clast sorting are absent (Shanmugam and Benedict, 1987; Loucks and Sarg, 1993). The source of calcareous material for these deposits likely comes from up-dip on the Horeshoe Atoll. Some of the allochems present within WKST and PKST beds are readily identifiable, but this is not always the case. This varying degree of preservation and taphonomic alteration may indicate multiple sources of allochem material.

Grainstones within the Martin County core occur as thin beds up to 6 inches thick. These beds are marked by scoured basal contacts, and can exhibit variable sedimentary structures including cross or massive bedding and normal grading. The tops of GRST beds are typically mottled, showing evidence of bioturbation or burrowing of fauna. Analysis of the grain size using the Dino-Lite handheld microscope reveals that the average size of allochems within this facies type is larger than 62.5 μm in diameter (Baldwin, 2016). These allochems exist as a carbonate sand derived from the abrasion of skeletal material. The degree of erosion of the sand impedes identification of the parent fossil material. Occasional laminations of siliciclastic clay and silt and pyrite can be found within GRST beds.

In contrast to WKST, PKST, and DOL, the GRST typically feature basal scour marks, normal grading, and uniformly small allochem grain size. As a result, GRST are interpreted to be deposited by turbidity currents. Allochthonous material derived from the Central Basin Platform and Horseshoe Atoll comprised the calcareous component of these facies. Beds with normal grading and scoured basal surfaces follow those of the Bouma sequence model, which describes low-concentration turbidity currents (Shanmugam, 1997). The erosive, turbulent flow scours out the sea floor as the gravity flow moves downslope, generating an irregular base and normal grading as flow velocity declines.

Carbonates with elevated magnesium and calcium content were interpreted as the DOL facies. This facies type has average calcium and magnesium content of 21.41% and 4.11%, respectively (n=36). Internally, beds of DOL are massive, with a cryptocrystalline texture. X-ray diffraction measurements supplied by Core Laboratories reveal that some

intervals contain up to ~68% dolomitized matrix. The matrix of a DOL from the Martin County core is predominantly ferroan dolomite, with residual calcite and a few pyrite crystals. Fossil fragments are occasionally present, but widely scattered throughout the crystalline matrix. Most fossils within the DOL show evidence of replacement by diagenetic silica. Some thin sections of DOL contain burrows that have been filled in with remineralized euhedral or subeuhedral ferroan dolomite. Several grains of glauconite were found across two thin sections, too. Vertical fractures, some containing secondary mineralization, are representative of the DOL facies type.

Dolostone intervals are inferred to be hardgrounds that form during periods of slow sediment accumulation, when the basin floor is starved of inputs. Seawater circulating through sediments results in cements precipitating out of the water column and lithifying the underlying sediment (Flügel, 2004). Cements commonly found in hardgrounds include high magnesium calcite and aragonite, which can be diagenetically altered to dolomite and calcite, respectively. Diagenesis during burial can impact the alteration of the matrix to dolomite. Alternatively, expulsion of seawater enriched in Mg^{2+} (during the conversion of smectite to illite) from pore spaces can result in dolomitization as burial depth and temperature increases; however, this model may require rapid burial. Other models for dolomite formation typically include the mixing of chemically distinct fluids, such as meteoric water-seawater mixing or evaporitic brines permeating carbonates. These models require hydraulic head, which then drives the movement of fluids. Burial dolomitization is interpreted to be the model that best fits this environment, where Mg^{2+} is supplied by clay alteration and transported by advecting pore water into a substrate absent of active sediment accumulation (Flügel, 2004).

There are two minor facies types present with the Midland Basin, Diagenetic Mineralized Beds, or "DMB" and a "Mixed" facies type. These are less pervasive within the Martin County core compared to the Upton County core (Baldwin, 2016). The beds of DMB in Upton County are typically very thin, on the order of less than 6 inches thick, and finely interlayered with BMR beds. Key characteristics of the DMB lithofacies type include pervasive dispersed or peloidal pyrite, phosphate nodules, and to a lesser extent, glauconite. The DMB facies type is absent in the Martin County core.

The Mixed facies type was first described by Baldwin (2016) in the Upton County core from the southern Midland Basin. This facies type is characterized by convolute, intercalated beds of mudrocks and carbonates. Within the Martin County core, carbonate sands and intraclasts are intermixed with a BMR-2 matrix. The chemical composition resembles that of BMR-2, with variable concentrations of Al, K, Ti, and Ca, all of which are dependent on the spot that the analysis was performed. There are three examples of this facies type in the Martin county core. The thicknesses range up to 2 ft. Trace element concentrations show no aberrations in enrichment or depletion in comparison to other facies types.

Other authors (Hobson et al., 1985) have found deposits similar to the Mixed facies type. Carbonates with allochthonous allochems were interpreted to have been deposited via soft-sediment deformation, but no mechanism was explicitly proposed. Multiple mechanisms exist for the explanation of soft-sediment deformation, including slope instability, seismic shaking, dewatering, or pore pressure changes due to regressions (Silva and Booth, 1984; Alves, 2015). However, identification of the exact mechanism likely requires either outcrops or 3D seismic data (Silva and Booth, 1985;

Alves, 2015). Slumping may be a possible explanation for mechanism, given the propensity of this environment for debris flows and turbidites (Figure 4.6). Another explanation for deformation is thrusting due to the creep of up-dip sediments (Schlager and Reijmer, 2009).

4.2 Lithostratigraphy

Formations tops were supplied with the Midland Basin data package delivered to UK by Pioneer Natural Resources. These were used in conjunction with petrophysical data to separate the Wolfcamp core into two basic formations, the Wolfcamp D (WC-D) and Wolfcamp C-2 (WC-C2). Other cores acquired from the Midland Basin included part of the underlying Strawn Formation, but the Martin County core was collected from just above the Wolfcamp D-Strawn boundary and only 6 inches of Strawn was delivered to UK. Since very little of the Strawn was provided, no interpretations will be attempted on its character and history. The WC-D is separated into three subdivisions, the Lower, Middle, and Upper WC-D, based on variations in vertical variability in facies stacking patterns and bulk geochemistry.

The Lower Wolfcamp D is ~143.5 ft thick (387.6 – 244.1 ft). It is predominantly composed of the GMR and BMR-2 facies types, with normalized abundances of 48.6% and 30.4%, respectively (Figure 4.1). Carbonates (PKST, WKST, and GRST) are poorly represented, with total abundances reaching 13.1%. These facies are mostly concentrated at the top of the Lower WC-D, where there are relatively thick packages of carbonates compared to the rest of this interval. Occurrences lower in the core are expressed as thin beds $\leq$6 in thick. The Mixed facies type is present only once, and thus has an abundance

of 1.4%. Gray mudrocks of the Lower WC-D are typically greater than 5 ft thick, or they occur as thin beds that are interlayered between BMR-1 and BMR-2 beds (Supplemental Figure 2). As previously mentioned, the transition from the Lower WC-D into the Middle WC-D is marked by a significant increase in the thickness of PKST and WKST, moving vertically up section.

The Middle Wolfcamp D is ~133 ft. thick, located between ~111.1 and 244.1 ft. in the core. This interval of the WC-D contains the highest degree of facies variability and stacking patterns of the whole core. Abundances of GMR decrease concomitant with an increase in BMR-1 (Figure 4.1). Packstones and WKST beds are markedly thicker than those of the Lower WC-D, ranging up to 0.3 m thick. Beds of the DMB facies appear only twice in the whole core, with both occurrences in the Middle WC-D. Dolostones occur in this interval for the first time as well. We interpret a repetitive (cyclic) vertical facies stacking pattern in the Middle WC-D. The ideal cycle ranges from 25 – 39 ft thick. Each cycle begins with BMR-1, which is overlain by successive BMR-2 and GMR beds. Moving up-section, the GMR beds are interbedded with PKST, WKST, GRST, and DOL facies types, typically < 3 ft thick, and bracketed by BMR-2 on the tops and bottoms. Not every succession contains a DOL bed, but there is always some form of carbonate facies type present. Within the Middle WC-D, there are four of these cycles; only one lacks a DOL interval. The high variability of facies within this section of the core is a key characteristic of the Middle WC-D for the Martin County core; no other interval shows as much variation.

The Upper WC-D is marked by an absence of DOL beds, as well as a significant increase in BMR-1 facies. It is approximately 68 ft long (111.1-43.3 ft) and has the

highest proportion of BMR-1 (34.5%) in the entire Martin County core (Figure 4.1). The abundance of the GMR facies is significantly lower compared to the Lower and Middle WC-D (~11%). This is concomitant with an increase in BMR-2, which constitutes ~36.1% of the Upper WC-D. The proportion of carbonate facies types shifts in Upper WC-D, such that WKST are essentially absent (0.26%) and the abundance of PKST and GRST has increased to 9.5% and 5.3% respectively. The Upper WC-D contains the largest amount of the MIX facies, ~2.9% of the sub-interval. Three cycles are identified in the Upper WC-D. The carbonates that are intercalated with BMR-2, and to a lesser extent GMR, beds are typically thin-bedded GRST. Packstones within the Upper WC-D are thicker than those found in underlying intervals, typically on the order of 1-2 ft. The Upper WC-D transitions into the WC-C2 at 43.4 ft, where the dominant facies type shifts to BMR-2.

The WC-C2 interval of the Martin County core is 43.3 ft in length. While not as much section is available with which to study the WC-C2, it is clear from the core that BMR-2 is the principal facies present, with an abundance of ~69.2% (Figure 4.1). Black Mudrock 1 and GMR are also present, but at significantly lower amounts (~12% each). Where carbonates are present, they are thinly bedded GRST; thick packages of WKST or PKST like those present within the WC-D are absent. Dolostone beds are represented, with three occurrences towards the top of the section. While more core would be required in order to make a detailed interpretation, a basic generalization of the vertical stacking patterns of the WC-C2 can be made here. Within the 43.3 ft. of core supplied, the increase of BMR-2 and the vertical succession of facies suggests that BMR-2 beds

replace those of GMR within the WC-D as the layers that are intercalcated with carbonates.

The WC-D can be described and partitioned into sub-intervals based on variations in the abundances of facies types, as well as changes in the vertical stacking patterns. The dominant facies type of the Lower WC-D is GMR. This trend shifts moving vertically through the core until BMR-2 becomes the prevailing facies of the Upper WC-D (Fig. 1). While the WC-C2 has the most BMR-2, it is also the thinnest sub-interval present within the core and thus harder to accurately describe. Assuming that the stacking trends observed prevailed through the WC-C2, then it can be said that BMR-2 is the dominant facies type. The Upper WC-D contains the highest proportion of BMR-1 and the Middle WC-D exhibits the largest variation in facies stacking patterns.

4.3 Inorganic Geochemistry

Geochemical analysis of the Martin County core at the 2-in scale resulted in a high-resolution dataset of 2,169 sample points and 4,338 total major and trace elemental analyses. This approach assisted in the fine-scale determination of facies variability, as macroscopic examination alone could lead to the misidentification of a facies type. Comparison of the gamma ray log and lithologic descriptions to the geochemical data showed consensus and good correlation among the datasets.

The major elements of interest were silicon, aluminum, calcium, potassium, titanium, magnesium, sulfur, and iron. These elements are indicative of the main rock forming minerals such as quartz, clays, feldspars, calcite, dolomite, pyrite, and ferromagnesian silicates. Trace elements of concern include molybdenum and chromium;

these are affected by changes in the redox conditions (Tribovillard et al., 2006; Algeo and Rowe, 2012) in the Midland seaway during the deposition of WC-D and WC-C2.

The chemostratigraphic plots generated with XRF data illustrate the high-frequency facies variability that characterizes within the Martin County core (Supplemental Figure 1). The sub-interval with the least amount of chemical variability occurs from 0 – 43.5 ft, which is the WC-C2 interval. The Middle WC-D shows the highest degree of variation in the chemostratigraphic plots, reflecting that the Middle WC-D contains the most variable facies stacking patterns.

Within the Lower WC-D, several trends can be identified. Aluminum, potassium, and titanium wt. % strongly covary moving up-section. Any deflections toward lower values are directly related to the presence of interbedded carbonates within thicker beds of GMR. Calcium values in the Lower WC-D are highly variable, due to the wide range in composition for GMR beds. There are no obvious long term trends for %Si through the Lower WC-D, but %Ca gradually decreases over time. Towards the top of the Lower WC-D (281 – 273 ft.), %Al and %Ti covary, but %K does not. In this interval %Al and %Ti increase slightly, decrease slightly, and then spike upwards. Molybdenum and chromium concentrations covary within the BMR-1 facies, and the gamma ray log also tracks these trace metals.

The Middle WC-D show the highest degree of variability of geochemical data in the Martin County core. Long term trends are harder to distinguish within this sub-interval due to the effect of the high frequency shifts in the geochemistry, reflecting the cyclicity in the lithofacies. However, the most apparent long term trend lies in %Ca values, which decrease slightly moving toward the top of the Middle WC-D. In general,

%Al, %K, and %Ti covary within the Middle WC-D. However, the concentration of these elements declines in the BMR-1 facies, which exhibits higher %Si. In BMR-2 and GMR, %Si will covary in step with %Al, %K, and %Ti. Spikes in %Ca, and to a lesser extent %Mg, can be traced to the interbedded WKST, PKST, GRST, and DOL intervals, although beds of GMR typically show only slightly elevated %Ca relative to the other mudrocks, due in part to aluminum-rich clays contributing to the mineral matrix.

The transition from the Middle to Upper WC-D marks a shift in the %Ca curve. While the Middle WC-D contained high frequency variation in the geochemical data, the Upper WC-D shows relatively low %Ca, if the abrupt spikes caused by carbonate beds are ignored. The covarying trends among %Al, %K, and %Ti continues in the Upper WC-D, as well as the subtle inverse relationship for %Si with respect to BMR-1 composition. The lower half of the Upper WC-D shows a slight decrease in %Al, %K, and %Ti, followed by a slight increase. The %Si curve shows the opposite trend, shifting to higher then lower values (Supplemental Figure 1). Approximately halfway through the Upper WC-D, the curve for %Si stabilizes and the degree of variability decreases. Variability in %Mo and %Cr also decreases up-section in the Upper WC-D. The curve for %Mg shows no long-term trends, with very few spikes that align with DOL beds.

4.4 Organic Geochemistry

Stable isotope data collected from the Martin County core is presented as a cross plot of a ratio of carbon to nitrogen (C:N) against $\delta^{13}C$ ‰, separated by facies type (Figure 4.4). A majority of the samples (~61%) have C:N values less than 10, an indication that most of the organic matter is derived from marine sources (Meyers, 1997).

Carbonate facies types (WKST, PKST, and GRST) were grouped and are represented as CARB on Figure 4.4. Black Mudrock 1 facies have molar C:N ratios above 10 and have $\delta^{13}C$ values of ~-27 to -26‰. Values for BMR-2 are more varied, with $\delta^{13}C$ values ranging from -25 to -27.5‰ and average C:N ratios of ~8 (n=14). Gray mudrocks are similar to BMR-2, with $\delta^{13}C$ values ranging from -25 to -28‰. The C:N data for GMR have an average value of 9.9 (n=12). These trends may suggest that organic material in BMR-1 facies is derived from more terrigenous sources, in comparison to BMR-2, GMR, and CARB facies. Alternatively, denitrification of organic material results in higher C:N, due to microbial processes converting available nitrogen into molecular nitrogen (N_2), a process known to take place in anoxic, marine environments (Algeo et al., 2008). The variability in BMR-2 and GMR C:N values indicates that these facies have a higher proportion of marine-derived (algal) organic material.

The dominant maceral type found throughout the WC-D and WC-C2 is alginite, reflecting the marine origins of the organic matter (Chapman et al., 2015). No trend was found between higher TOC intervals and changes in maceral type composition, thus suggesting that BMR-1 facies does indeed contain abundant algal organic matter and that denitrification may be impacting C:N. Other factors influencing C:N ratios may include detrital organic matter being flushed into the basin due to runoff. This plays a role later, specifically with regards to the Re-Os geochronology discussed later.

Principle component analysis (PCA) was conducted on the XRF dataset in order to determine the variance in the data. The first (PC1) and second (PC2) components account for ~80% of the total variance, with PC1 and PC2 accounting for 59.4% and 20.6% of the variance, respectively (Figure 4.5). Principle component 1 loads strongly

positive for the major elements %Si, %Al, %K, and %Ti, with weaker positive loadings for %S, %Fe, %Mo, and %Cr. Calcium shows a strong negative loading for PC1. This leads to the interpretation that PC1 is a relative proxy for mineralogy, where positive scores indicate siliciclastic rocks and negative score reflect carbonates. The second principle component shows a strong positive loading with elements associated with bottom water redox conditions (%Mo, %Cr, %S, and %Fe), a negative relationship with elements indicative of terrigenous inputs %Al, %K, and %Ti), and a weakly positive loading for %Ca. As a result, PC2 is interpreted to represent the variation in redox conditions (positive values reflect a strongly reducing environment) during deposition.

The frequency and magnitude of shifts in the PC1 curve demonstrate changes in lithofacies, due to PC1 representing variance in the major elements that constitute minerology. Strong peaks where positive values of PC1 and PC2 align are associated with BMR-1 packages. Black mudrock 2 facies are represented by lower PC1 values and PC2 values near zero, compared to BMR-1. This is interpreted to be a reflection of the different redox and bottom water oxygen content within conditions under which the BMR-1 and BMR-2 facies were deposited. Carbonate facies (WKST, PKST, GRST, and DOL) are associated with negative PC1 and PC2 values. The GMR facies is characterized by either slightly negative values or score of zero for both PC1 and PC2 (Supplemental Figure 3). Throughout the Lower WC-D, the PC1 curve is slightly positive, with occasional deviations due to the presence of thinly bedded carbonates. Principle component 2 in the Lower WC-D is typically zero or negative, with occasional positive excursions due to interbedded BMR-1 facies. This is due to the high proportion of BMR-2 and GMR lithofacies types. The Middle WC-D is represented by high frequency

deflections in the PC1 curve, reflecting the greater variability in lithofacies found in this interval. The plot of PC2 through the Middle WC-D is more "sawtooth" in shape, with positive values occurring during BMR-1 intervals and PC2 values decreasing through the cycle until the next BMR-1 bed (Supplemental Figure 3). Principle component 1 values for the Upper WC-D are similar to those found in the Middle WC-D, in that the values are on average more positive with deflections caused by the occasional CARB or GMR bed, and PC2 values show narrow peaks with broad descending limbs and local minima corresponding with stratal cycles.

4.5 Re-Os Geochronology

The measured Re and Os concentrations and isotopic ratios ($^{187}Re/^{188}Os$ and $^{187}Os/^{188}Os$) are shown in Table 1. Osmium abundances taken from the three cores range from 1.095-1.293 ppb, and Re values vary from 68.9-139.9 ppb. These values are larger than present day Re and Os concentrations of the upper crust, which are 0.39 ppb and 0.05 ppb, respectively (Esser and Turekian, 1993). The calculated isotopic ratios for $^{187}Re/^{188}Os$ vary from 377-835, all of which are greater than the current $^{187}Re/^{188}Os$ ratio for present day continental crust, which ranges from 42-48. The average $^{187}Os/^{188}Os$ value for present day continental crust is approximately 1.26 (Esser and Turekian, 1993), significantly lower than the range of $^{187}Os/^{188}Os$ values for the cores (2.61-4.85). Whole rock ages calculated from the BMR-1 samples analyzed yield an absolute age of 300 ± 18 Ma (MSWD = 63) and an initial $^{187}Os/^{188}Os$ value of 0.66 ± 01.15 (Figure 4.7).

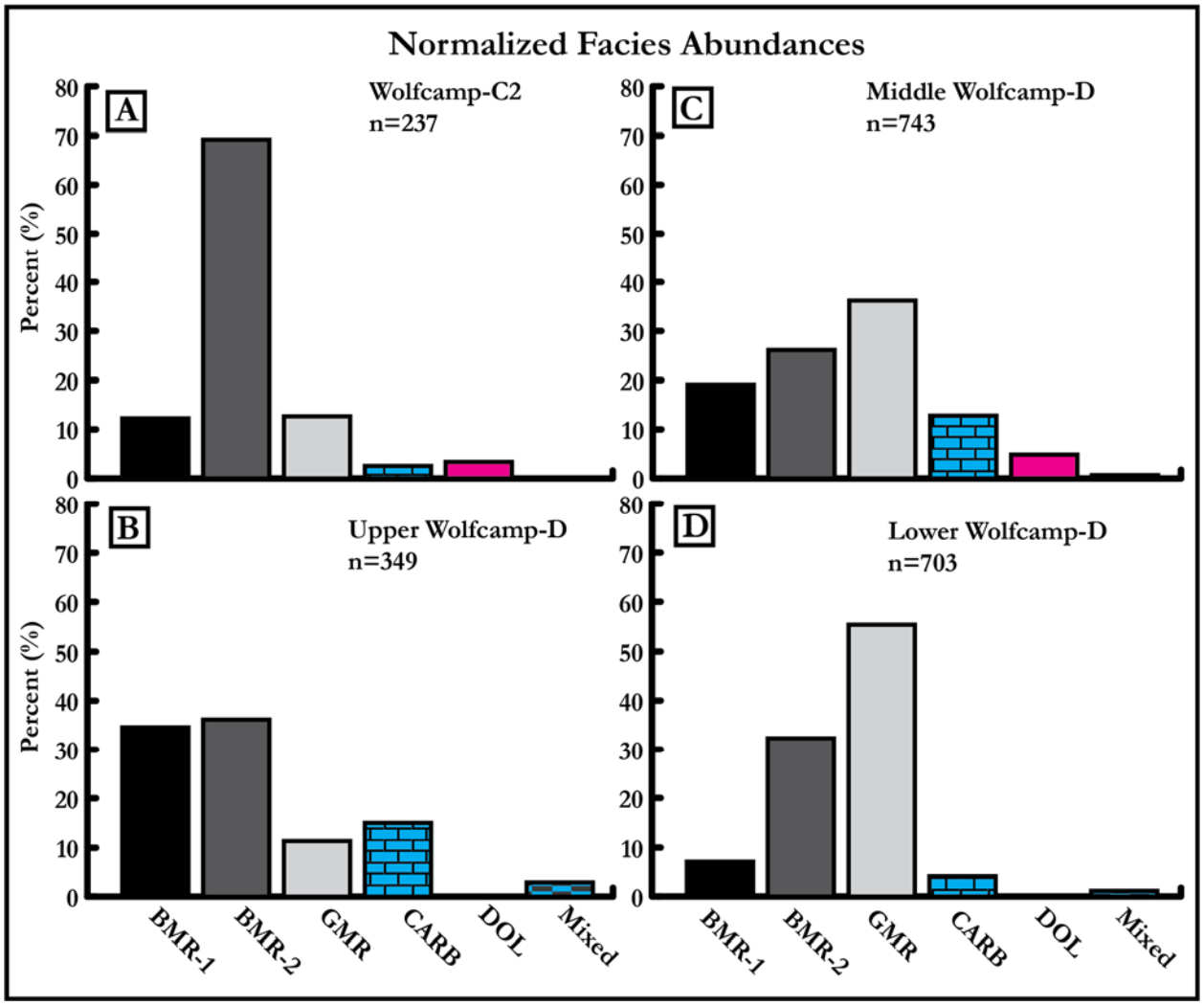

Figure 4.1. Normalized Facies Abundances for the Wolfcamp D and C2 subintervals. The normalized distribution of facies types for each subinterval. Quantities were calculated using facies designations assigned to each XRF data point. Wackestones, packstones, and grainstones are grouped into "CARB" for simplicity. A) Wolfcamp-C2, B) Upper WC-D, C) Middle WC-D, D) Lower WC-D.

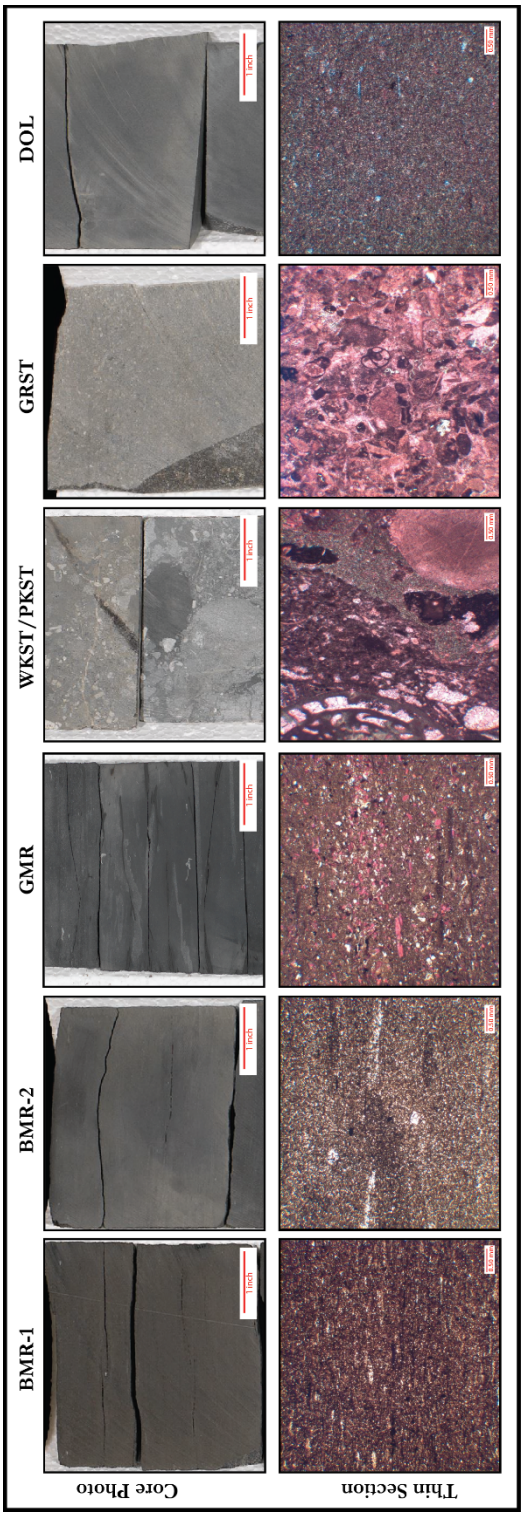

Figure 4.2. Major Lithofacies in Hand Sample and Thin Section
Photographs of the major facies types present in the Martin County core. Top photos are high-resolution photographs of slabbed core, bottom photographs are of thin sections. From left to right the lithofacies are BMR-1, BMR-2, GMR, WKST/PKST, GRST, and DOL. Thin section photographs were supplied by CoreLab.

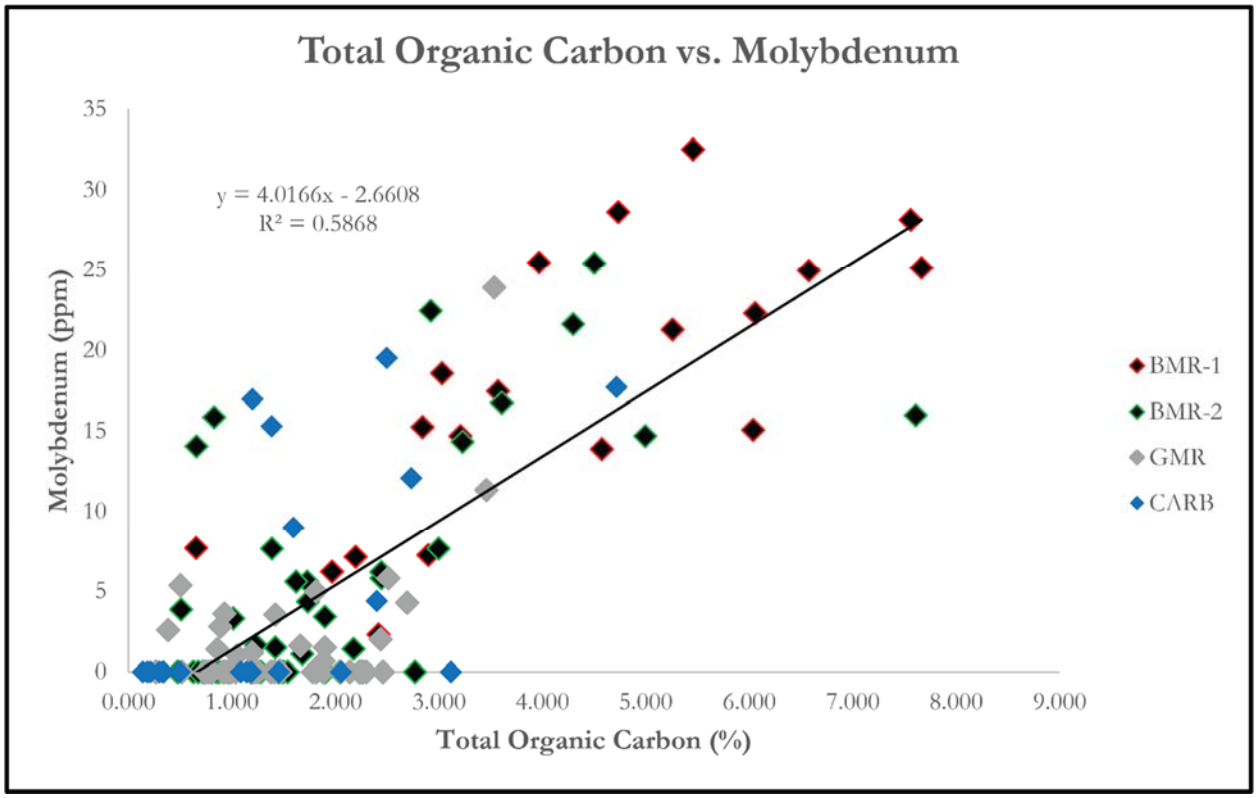

Figure 4.3. Total Organic Carbon versus Molybdenum.
Cross plot of Mo and TOC, with linear regression, for the WC-C2 and WC-D of the Martin County core. The regression includes all facies types. Wackestones, packstones, and grainstones are grouped into the "CARB" category.

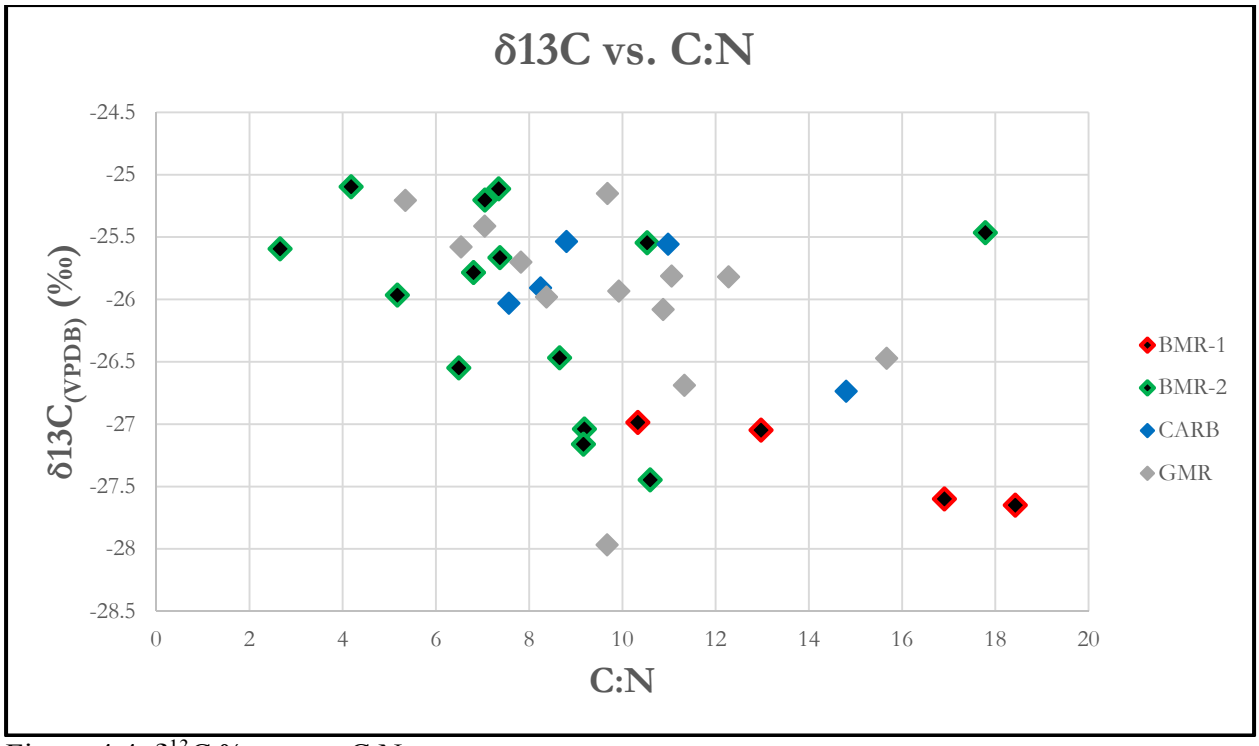

Figure 4.4. $\delta^{13}C$ ‰ versus C:N.
Stable isotope data separated by lithofacies, and includes data taken from the whole length of the core. Marine-derived organic material typically has a C:N value less than 10. Terrigenous sources yield ratios <15. Ratios in between 10-15 indicate either mixing of organic matter from different sources or diagenetic alteration (Meyers, 1997).

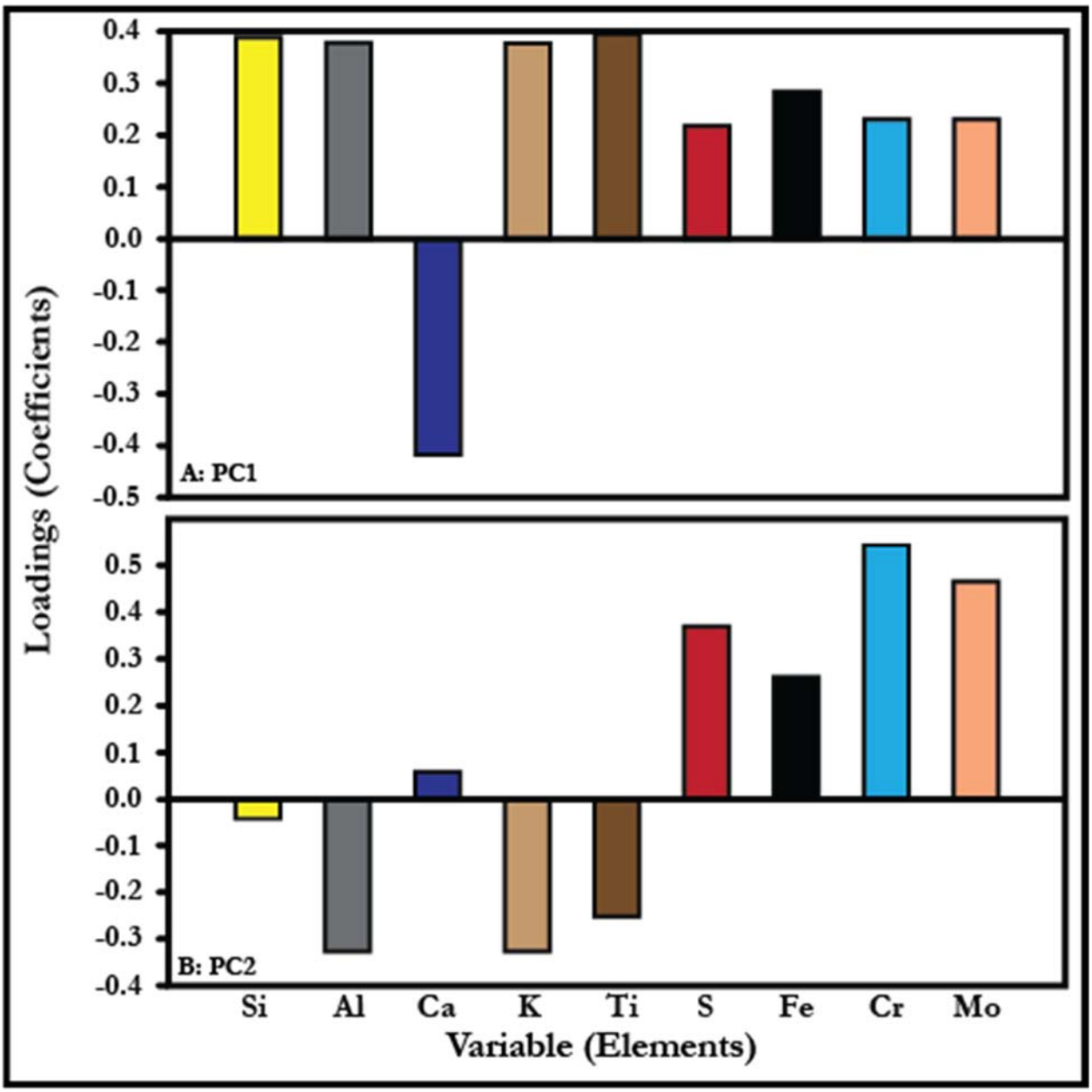

Figure 4.5. Principle Component Analysis Loadings
Plots of loading coefficients by variable (chemical elements) for the first two principle components. A) Principle component 1 (PC1) loads positively with the key constituents of mudrocks (Si, Al, K, Ti) and trace metals (Mo, and Cr), but negatively with Ca. Principle component 2 (PC2) loads positively on elements sensitive to redox conditions (Fe, S, Cr, and Mo), and negatively with those associated with terrigenous material, (Si, Al, K, Ti). This suggest that periods of anoxia correspond with less runoff.

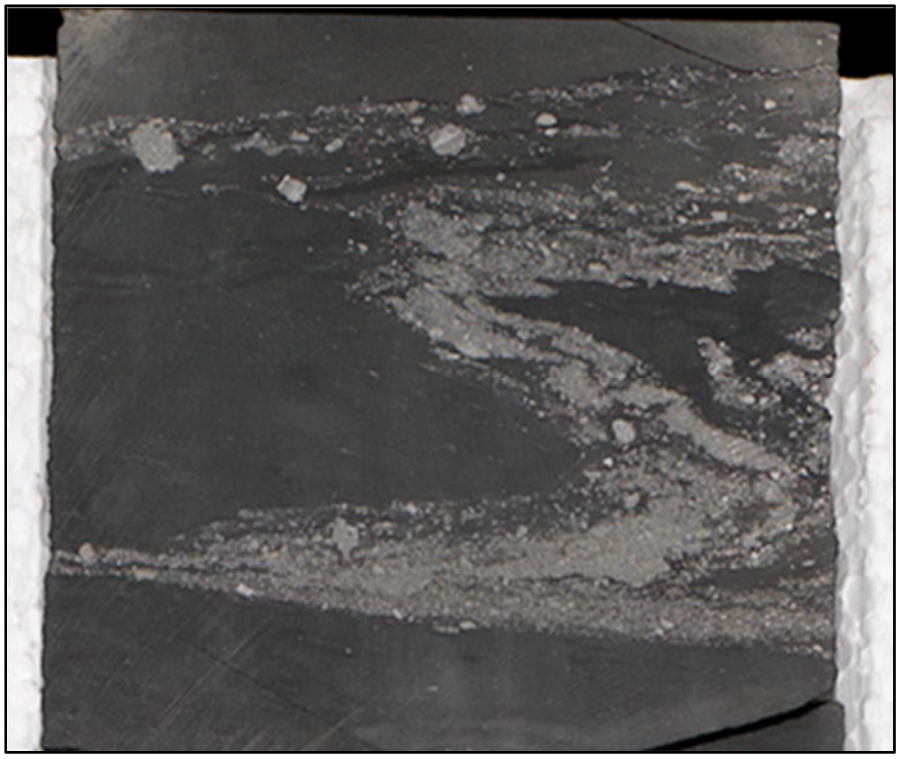

Figure 4.6 Mixed Facies type
Photograph of the 1/3 slab of core, showing the convoluted structure of the Mixed facies type. Disrupted bedding could potentially be caused by slumping and thrusting caused by up-dip creep.

Sample	A-1	A-2	A-3	H	U
Os Conc. (ppb)	1.156	1.162	1.153	1.293	1.095
188Os (moles/g)	6.088E-13	6.122E-13	6.041E-13	5.583E-13	5.494E-13
Re Conc. (ppb)	70.3	68.9	72.4	139.9	76.3
187Re (moles/g)	2.36E-10	2.31E-10	2.43E-10	4.66E-10	2.56E-10
187/185 error 2sigma (abs)	0.000292	0.000495	0.003014	0.000404	0.001174
187Re/188Os	**388.1**	**377.9**	**402.5**	**835.3**	**466.8**
187Re/188Os error 2sigma (abs)	**0.0041**	**0.0032**	**0.0064**	**0.0070**	**0.0140**
187Os/188Os	**2.61**	**2.61**	**2.66**	**4.85**	**2.94**
187Os/188Os error 2sigma (abs)	**0.004**	**0.003**	**0.006**	**0.007**	**0.014**

Table 4.1. Re-Os isotopic data

Five samples were collected from the donated cores, 3 from the Martin County core, and 1 each from the Midland and Upton County cores, respectively. Samples were prepared and run on a Thermofischer Triton multicollector following Rasoazanamparany et al. (2016).

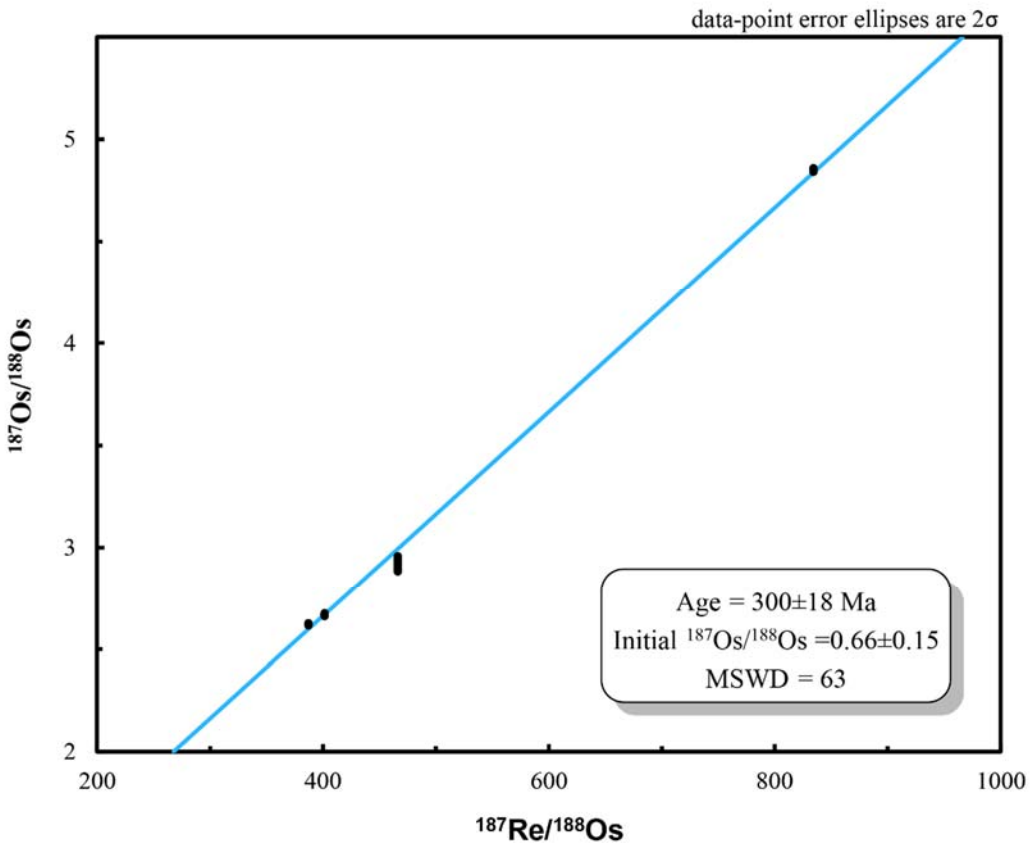

Figure 4.7. Re-Os Isochron for Martin, Midland, and Upton County cores
The samples run result in a depositional age of 300 ± 18 Ma. Error bars were significantly enlarged in order to be visible. The MSWD = 63 may be due to detrital Os (see text for further details).

CHAPTER FIVE: DISCUSSION

5.1 Depositional Controls on Lithofacies

The nine lithofacies types identified in the Martin County core were deposited by either a specific mechanism or a series of linked processes. During the Late Pennsylvanian, the influence of global climate on glacioeustatic sea-level is hypothesized to impact depositional mechanisms in marine basins. In addition, understanding how marine facies develop in the Midland Basin has important implications for petroleum resources, particularly source rocks. Accordingly, a key focus of this study is to ascertain the paleoenvironmental conditions that may have been responsible for the development of organic-rich lithologies. Passey et al. (2010) noted that production, preservation, and dilution are critical processes that control the deposition of petroleum source rocks. Prior research in the Midland Basin (e.g., Baldwin, 2016; Ryan, 2016) made linkages between stratigraphic and geochemical cycles identified in sub-surface datasets and global sea level curves (e.g., Ross and Ross, 1987). We used the framework of Ryan (2016) to interpret lithofacies in Martin County in the context of sea level fluctuations. Figure 5.1 is a "type cycle" interpreted from the Middle WC-D paired with an individual, hypothetical eustatic sea level cycle. Lithofacies were matched to corresponding parts of an idealized sea level curve. Interpreted depositional mechanisms and environments for each lithofacies are shown in Figure 5.2. These inferences were then applied to the rest of the core, and a relative Midland Basin sea level curve was interpreted and applied, as shown in Supplemental Figure 3.

Sea level lowstands are interpreted to reflect accumulation in a restricted, anoxic basin which provided the necessary conditions for the deposition of the BMR-1. Molybdenum (Mo) has previously been used in combination with total organic carbon (TOC) as a proxy for bottom water recharge rates in modern oceanic basins (Algeo and Rowe, 2012). In oxygenated waters, Mo is conservative and stays in solution within the water column. Anoxic conditions result in the reduction and removal of Mo, where it is then incorporated into organic matter and the sulfide fraction of fine-grained pelagic sediment (Vorlicek et al., 2004). Therefore, in an anoxic environment marked by limited bottom water circulation, Mo and TOC tend to be positively correlated (Algeo and Maynard, 2004; Algeo and Rowe, 2012). The slope of the regression between Mo and TOC data can be used to infer the redox conditions and recharge rate of the basin (Algeo and Maynard, 2004; Algeo and Rowe, 2012). Basins with higher rates of bottom water recharge have higher Mo-TOC ratios, since higher rates bring more Mo from the open ocean into the basin, which can be stored in the sediment (Algeo and Rowe, 2012). Conversely, restricted basins have lower capacity for Mo recharge and Mo-TOC ratios are much lower. The Martin County core shows a positive correlation between Mo and TOC, where the slope of the regression equals ~4.01 (Figure 4.3). The slope of the regression line is similar to that of the Black Sea, a modern day silled basin that is anoxic and euxinic (Algeo and Rowe, 2012). Correlation coefficients for the Upton and Midland County cores are markedly higher compared to the Martin County core, likely the result of changing redox conditions moving along the strike of the basin from south to north (Baldwin, 2016; Ryan, 2016). Algeo and Heckel (2008) published values for Late Pennsylvanian black shales deposited on the Kansas Shelf during transgressions that

imply a strong connection existed between the LPMS shelf and Panthalassa, and this water source likely advected through the Midland Basin. Bottom water redox conditions are a key environmental factor impacting deposition, as these conditions dictate the preservation of organic matter in BMR-1 during lowstand intervals. Along strike variability within the basin is apparent, based on the interpretations of Baldwin (2016) and Ryan (2016). This is likely due to the proximity to channels, paleobathymetry, and proximity to the Horseshoe Atoll. The Upton County core was proximal to the Hovey Channel which connected the southern part of the Midland Basin to the Delaware Basin, as well as the Panthalassic Ocean (Algeo and Heckel, 2008). The Midland County core is situated more towards the basin depocenter, and as such records fewer grainstone turbidites (Ryan, 2016). Interestingly, the Upper WC-D for the Martin County core contains the highest abundances of BMR-1 throughout the section, whereas the Upton and Midland County cores do not record this trend (Baldwin, 2016; Ryan, 2016). Instead, BMR-1 peaks in the Lower WC-D for the Upton County core, and in the Middle WC-D for the Midland County core (Figure 4.1; Baldwin, 2016; Ryan, 2016). This trend is different than what is seen in the Midcontinent cyclothems of Kansas, when core black shales are deposited during transgressions of sea level. Upwelling during lowstands is interpreted to produce highly productive surface waters within the Midland Basin, which resulted in the deposition of high TOC sediments. Black Mudrock 1 facies contains phosphatic nodules and lenses and silicified *Tasmanites* cysts (Supplemental Table 1). Petrographic analysis revealed these algal cysts are likely the source of the high %Si content of the BMR-1 facies type (Baldwin, 2016). Schieber (1998) found that during

diagenesis, dissolved biogenic silica from radiolarians is re-precipitated into algal cysts, which can become a source of biogenic quartz silt and sand in shales and mudstones.

The BMR-1 facies type is also characterized by low %Al, %Ti, and %K content, elements which are interpreted as indicators of terrigenous flux, due to their common association in detrital clay minerals. Lower precipitations rates during lowstands are consistent with the reductions in the amount of terrigenous minerals found in BMR-1 facies. Lowstands occur concomitantly with local maxima of the PC2 curve, as PC2 loads negatively with Al, K, and Ti, which are indicative of terrigenous inputs and a proxy for continental runoff rates. Global circulations models of equatorial western Pangaea predict that precipitation rates would be primarily impacted moisture availability and surface temperatures (Heavens et al., 2015). Monsoonal circulation patterns created by the establishment of Pangaea would be suppressed by the decrease in differential heating between Pangaea and Panthalassa during glacial intervals. The reduction of monsoon strength would in turn be exacerbated by high-altitude glaciation of the Ancentral Rockies or Central Pangaean Mountains (Soreghan et al., 2014; Heavens et al., 2015). Pervasive aridity during glacial intervals occurs due to the narrowing of the Inter-Tropical Convergence Zone (ITCZ), as a result of the expansion of ice sheets (Soreghan, 1994). Taken together, higher levels of aridity and lower precipitation should create an environment marked by limited sediment transport from the continents to the ocean. Organic enrichment in sedimentary rocks is determined by three influences: production, dilution, and destruction (Passey et al., 2010). With the relatively low values of Al, Ti, and K in BMR-1 facies, a reduction in terrigenous inputs indicate a low probability of organic matter dilution at the Martin County core site. Lower fluxes of terrigenous

material from the continent would reduce the impact of dilution in this depositional environment. In addition, high rates of runoff would favor a strong pycnocline, inhibiting the efficacy of upwelling currents to deliver nutrients. The TOC and phosphate content of BMR-1 are not consistent with these conditions however. Rather, less continental runoff should favor a reduction in water column stratification, allowing for erosion of pycnoclines and more upwelling of limiting nutrients which allow photosynthetic plankton to thrive (Jaminski et al., 1998). Upwelling in the Midland Basin drives primary productivity, increasing the production of organic material, which is indicated by the presence of phosphate nodules and lenses. As runoff rates begin to increase at transition points on the sea level curve (e.g., tracking the switch from BMR-1 to BMR-2 deposition), phosphate nodules disappear; this is consistent with the influence of rainfall and wind on upwelling. This does not mean, however, that upwelling occurred everywhere equally throughout the Midland Basin; internal circulation can distribute nutrients in elongate aquatic basins. Additional subsurface datasets may help to resolve spatial variability in the upwelling signal.

Using the lowstand enrichment model as a base, the relative timing of deposition on the sea level curve for other lithofacies was determined (Ryan, 2016). Principle component 2 data shows a cyclical pattern, with BMR-1 facies coinciding with high PC2 values, which we interpret as sea level lowstands and a highly anoxic sea floor that aided in organic matter preservation. As the PC2 curve declines from maximum values, the proportion of BMR-2 increases. Gray mudrocks and carbonate intervals fit within minima within a PC2 cycle. The cyclical nature of the PC2 data reflects the changes in redox conditions that are associated with the progression of a sea level cycle as we interpret it.

Black Mudrock 1 is gradationally bounded above and below by beds of BMR-2 facies. Somewhat similar depositional conditions for BMR-2 prevailed for BMR-1, albeit with some important differences. Lower TOC in BMR-2 are attributed to several environmental and oceanographic factors, including lower rates of primary production, bacterial degradation of organic matter and bioturbation on the sea floor, and dilution by the influx of clay minerals. Dilution is believed to be linked to changes in continental runoff during BMR-2 deposition. For example, continental runoff is interpreted to have been higher during BMR-2 deposition, due to higher %Al, %Ti, and %K. An increase in precipitation is anticipated during times of transgression. However, during regressions it is expected that as sea level drops, incised valleys transport more terrigenous material. Black Mudrock 2 facies have lower average TOC values compared to BMR-1, but the maximum values are nearly equivalent (Supplemental Table 1). This is potentially caused by variable decomposition of organic matter due to bacteria, a process that is far less efficient in anoxic waters (Sageman et al., 2003). Photomicrographs of thin sections taken from BMR-2 facies show disrupted fabrics, potentially signifying bioturbation (Figure 4.2). These data are consistent with higher oxygen content on the sea floor during BMR-2 deposition, which partially explains the lower average TOC. High PC1 and low PC2 values are consistent with this process. Higher rates of continental runoff during early rising and late falling stages would also increase water column stratification, hampering organic enrichment of BMR-2. Phosphate nodules and lenses, a common indicator of BMR-1 intervals, are absent BMR-2 facies. These lines of evidence suggest that there was a reduction in primary productivity associated with upwelling.

Dolostone (DOL) intervals are interpreted to form as cement grounds *in situ*, during periods of maximum sea level rise and low sedimentation rates in the deep furrow of the basin. Interactions between bottom waters and pore fluids result in the precipitation of high-magnesium calcite and aragonite, forming a cement ground (Flügel, 2004). The formation of dolomite with respect to sea level change is debated in the literature. Most models that describe the formation of dolomite place an emphasis on subaerial exposure and circulation of meteoric water through carbonate platforms; this model and its setting are not applicable to the Martin County core site (Flügel, 2004; Al-Awadi et al., 2009). The diagenetic transition of smectite to illite can release Mg^{2+} into pore waters, which is then dolomitize carbonates during burial (Flügel, 2004). This burial model may explain how some DOL formed within the Martin County core. Not all carbonate facies are dolomitized, so there may be other environmental factors that result in some intervals being preferentially altered over others. More research is required to answer this question, as well as if DOL can be used as regional marker beds.

Facies deposited during sea level highstands include GMR, WKST, PKST, and GRST, corresponding to interglacial intervals. At these times, the prevailing mechanism of deposition was export of terrigenous material with respect to GMR. Transport of carbonate sediment occurred due to highstand shedding of allochems from the surrounding platforms and bioherms (Figure 1.1). Transitions between mudrock facies types are gradual and bed boundaries are commonly diffuse. This suggests progressive, rather than abrupt, changes in environmental conditions (bottom water redox, runoff, mass wasting), particularly between BMR-2 and GMR. In contrast to BMR-1, the GMR facies type contain low TOC content (μ=1.47%). This is explained by a decrease in

productivity, the presence of oxygenated bottom waters, and increased dilution from both terrigenous clays (represented chemically by %Al, %K, and %Ti) and lime mud, finely abraded shells, and macrofossil content, which are reflected in higher %Ca (Supplemental Figure 2). During interglacial periods, precipitation rates increased, leading to greater rates of runoff from the continents. A pulse of freshwater from the continents is interpreted to strengthen stratification in the Midland Sea, as this low density water mass floats above highly concentrated marine water, separated by a sharp halocline (Algeo and Heckel, 2008). Coupled with a strengthened halocline, sea surface temperatures would also be high, establishing a thermocline which would inhibit upwelling. Evidence of bioturbation in GMR facies is prevalent through most of the intervals, indicating that fauna were present and that bottom waters were at least partially oxygenated (Sageman et al., 2003). Oxygenated bottom waters contribute to the bacterial and faunal degradation of organic matter, thus reducing the organic preservation of GMR and resulting in these facies having low TOC content. Increases in continental runoff, as well as highstand shedding, during the deposition of GMR results in a higher flux of clays and carbonate allochems into the basin, diluting the organic content within GMR beds. This is supported by GMR facies having lower PC2 values as a result of GMR having less S, Fe, Mo, and Cr which load strongly positive, with regards to PC2 scores, and strongly negative in terms of Al, K, and Ti (Figure 4.5).

Carbonate facies types (WKST, PKST, and GRST) are closely associated with GMR in stacking patterns, implying some connection. Downslope transport of allocthonous carbonate material from basin-margin platforms is well-described in the carbonate stratigraphy literature (Schlager, 2005). Carbonate factories during highstand

intervals are active and platforms grow vertically into the photic zone, in order to facilitate photosynthesis for reef-building organisms. Erosion of the reef front and slope by wave action as sea level rises and floods the platform serves to transport calcareous detritus downslope, into adjacent basins (Schlager et al., 1994; Saller et al., 1999; Flügel, 2004). Highstand shedding of carbonate material into the adjacent basins by turbidity currents has been observed on the platforms of the Caribbean, Indian Ocean, and Great Barrier Reef (see Schlager, 2005, and references therein). Wackstones, PKST and GRST found in the Martin County core are interpreted to have been deposited via gravity flows, with WKST and PKST transported by debris flows and GRST by turbidity currents. Packstones and WKST lack erosive basal contacts, which are characteristic of laminar flow along the bottom of a sediment-rich, gravity driven flow. Other features of WKST and PKST that are shared with debris flows include projected clasts, inverse grading, and poorly sorted clasts (Shanmugam and Benedict, 1978). The lack of an erosional contact between these facies and overlying mudrock facies may imply that these deposits are transported during low velocity events. The size of the allochems present also suggests that these deposits are not transported long distances (Shanmugam and Benedict, 1978). The fine-grained debrites tend to be thicker and lack internal structure, compared to GRST facies which typically feature incomplete Bouma sequences. Grainstone facies also exhibit erosional scour surfaces at the base, as well as finer grains compared to WKST and PKST facies. The gravity flows represented by WKST and PKST likely reflected highstand shedding of carbonate reef material into the basin. During highstands, carbonate production in reef complexes would be active, resulting in the production of large volumes of material (Loucks and Sarg, 1983). This sediment would be predisposed

to erosion and transport via wave action and currents, leading to the transport of material during mass wasting events and gravitational flows. These debris flows interrupt background sedimentation, but do not necessarily erode previously deposited sediment (Loucks and Sarg, 1983). In contrast, GRST facies present indicate that the depositional process was a low-density turbidity current. This is inferred based on the presence of basal scour marks, a uniform sand-size sediment, and occasionally plane parallel laminae (Sanders, 1960). Dolostone facies, where present, are usually found stratigraphically below WKST, PKST, and GRST facies. This supports the notion that GRST are indicative of sea level highstand intervals, and DOL represent times of maximum sea level rise. In cases where this hypothesis does not seem valid, shorter or incomplete cycles may be present.

5.2 Stratigraphic Development

Deposition of cyclothems during the Late Paleozoic Ice Age (LPIA), and climate variability, has been studied in a number of basins across the globe (Boardman and Heckel, 1989; Rasbury et al., 1998; Saller et al., 1999; Feilding et al., 2008a, 2008b; Heckel, 2008; Greb et al., 2009; Eros et al., 2012; Isbell et al., 2012; Montañez and Poulsen, 2013; van den Belt et al., 2015). Understanding changes in global ice volume is key, as it is intrinsically tied to eustatic sea level change. The interpretation of the WC-D provided here was developed using current literature on the LPIA and cyclothems deposited during this time period (Montañez and Poulsen, 2013). The Wolfcamp D is interpreted to be equivalent to the Strawn, Canyon, and Cisco Formations found on the shelf. This is supported by biostratigraphic correlation of fusulinids to shelf strata, as well as basin-wide well log correlations completed by Pioneer Natural Resources (Waite et al.,

2015). A total of 13 sea level cycles were interpreted for the Martin County core, with 11 cycles contained within the WC-D (Supplemental Figure 3). Relevant studies for establishing a framework for WC-D deposition typically lack accurate age control, especially within the narrow time period (~10 Ma) that this study is concerned with.

Due to the paucity of literature that covers the Late Pennsylvanian stratigraphy of the Midland Basin, studies discussing contemporaneous horizons with precise ages provide the context required to develop an understanding of the WC-D. A relevant study for understanding late Pennsylvanian sea level change in the Permian Basin comes from the carbonate stratigraphy of the Central Basin Platform (CBP). Dating techniques applied to rocks collected from the CBP analyses indicate that deposition took place during the Desmoinesian to Virgilian (309-299 Ma) (Waite and Reed, 2014). Saller et al. (1999) used well log data, thin section analysis, and lithostratigraphy from the CBP to interpret 87 sea level cycles on the CBP; cycle boundaries were identified based on sedimentological clues of subaerial exposure (e.g., karstification, paleosol development, etc.). Radiometric dating of paleosol horizons collected from a CBP core established a mean cycle length of 143 ± 64 ka, similar to the duration of the eccentricity Milankovitch cycle (Rasbury et al., 1998). This high resolution age dating allows for the correlation of CBP cyclothems to other basinal cycles of the Demoinesian, Missourian, and Virgilian (309-299 Ma). Northern hemisphere glaciation of the Pleistocene has been shown to be connected to the eccentricity cycle of ~100 ka (Clark et al., 1999). Changes in the eccentricity cycle result in a substantial change in the global climate (Clark et al., 1999). Therefore, the 100 ka cycle is an important driver of high-frequency, glacioeustatic sea level change and deposition, not just within the Midland Basin, but across the globe.

This climate forcing due to eccentricity is seen in other contemporaneous basins that have robust age control (Saller et al., 1999; Eros et al., 2012).

Another useful study that provides context for sea level change in the late Pennsylvanian comes from the Donets Basin of Ukraine (Eros et al., 2012). Stratigraphic analysis of limestones and coals coupled with U-Pb measurements of tonsteins resulted in an onlap-offlap curve for the Donets Basin (Eros et al., 2012). Cycles in the Donets Basin were found to have three periodicities: ~140 ka, ~400 ka, and ~1.6 ma. The Donets Basin experienced relatively uniform subsidence during the Late Pennsylvanian, allowing for the correlation between its onlap curve and the 12 North American cyclothems described from the Midcontinent region (Heckel, 2008; Eros et al., 2012). The sea level curve produced by Ross and Ross (1987) for North America is commonly used as a reference in studies concerning the LPIA (Waite, 2015). The sea level curves presented from the US Midcontinent, the Donets Basin, and our interpretation of the Midland Basin shares several features in common, including:1) the Late Desmoinesian into the Missourian is characterized by a long-term transgression; 2) a long-term highstand during the Missourian, coupled with the highest frequency of sea level variability; and 3) a sea level regression into the Virgilian, leading to a reversal in the WC-C2 and decrease in variability (Ross and Ross, 1987; Saller et al., 1999; Eros et al., 2012).

The Lower WC-D is interpreted to record a long-term transgression with four high-frequency sea level cycles superimposed upon the longer trend. The four cycles (cycles #10-13) were interpreted based on the presence of thin-bedded carbonates (WKST, PKST, and GRST) intercalcated with GMR facies, and BMR-2 packages. Facies abundances of the Lower WC-D agree with this interpretation, and are consistent with a

long-term sea level rise absent of deep and sustained lowstands. The Lower WC-D is predominantly composed of GMR with some accessory BMR-2, facies that are interpreted to be indicative of highstand and initial transgressive-regressive intervals, respectively. This is likely representative of a relatively deepwater conditions in the basin, as well as more continental runoff and shedding of carbonate allochems from the surrounding platforms. Within the Lower WC-D, the proportion of BMR-1 relative to other facies type is at the lowest. Bed thicknesses decrease moving up-section through the Lower WC-D, which is consistent with a change in stacking patterns transitioning into the Middle WC-D. This trend is similar to those seen in the Midcontinent, the Central Basin Platform, and the Donets Basin onlap-offlap curves, where bed and cycle thickness decrease moving out of Lower WC-D time (Ross and Ross, 1987; Saller et al., 1999; Eros et al., 2012).

The published literature has established that the Missourian stage of the Late Pennsylvanian exhibits the largest variability in sea level magnitude and frequency (Eros et al., 2012; Waite, 2015). This stage is interpreted to be time-equivalent to the Middle WC-D, based on the high frequency variability observed in facies abundances (Figure 4.1). The Middle WC-D also demonstrates the most repetition in terms of cyclic lithofacies stacking patterns. Four cycles were interpreted within the Middle WC-D (Cycles #6-9, Supplemental Figure 3). Three of the cycles (#6, #7, and #9) include DOL facies, but in cycle #8 DOL is absent. All of the cycles in the Middle WC-D feature either WKST, PKST, or GRST facies types. The high variability of facies present in this interval indicates that the Middle WC-D contains the best representation of true cyclicity within the Martin County core.

The Upper WC-D is represented by three cycles (Cycles #3-5, Supplemental Figure 3). Facies stacking within this interval is characterized by a significant increase in BMR-1 and BMR-2 (Figure 4.1). Other changes in stacking patterns include the absence of DOL, and a shift from the deposition of WKST, PKST, and GRST to solely GRST facies. This change in depositional mechanisms, from debris flows and turbidites to predominantly turbidites may indicate the beginning of sea level regression. As sea level drops, the abundance of highstand carbonate (WKST and PKST) should decrease. The increase in both BMR-1 and BMR-2 may indicate a gradual long-wavelength regression moving through the Upper WC-D. This interpretation is consistent with the change in facies stacking patterns and is corroborated by the Ross and Ross (1987) and Donets Basin sea level curves, both of which suggest a regression towards the end of the Pennsylvanian (Figure 2.2) (Eros et al., 2012). The Wolfcamp C2 (WC-C2) is represented by only ~40 feet of core, but some generalizations may be made about this section using the Ross and Ross (1987) sea level curve. The dominant facies type of the WC-C2 in the Martin County core is BMR-2. The Ross and Ross (1987) curve depicts a relatively small transgressive-regressive cycle moving through the Virgilian into the Nealian stage (Montanez and Poulsen, 2013). While not all of the WC-C2 was recovered and delivered to UK, an increase in BMR-2 is consistent with relatively high long-wavelength sea levels. The frequency of short-wavelength sea level change also decreases moving through the WC-C2, explaining the change in distribution of facies. The eleven cycles interpreted from the Wolfcamp D generally agree with the findings of previous studies (Heckel, 2008; Eros et al., 2012) in which twelve cycles were interpreted for the midcontinent and the Donets Basin.

5.3 Re-Os Geochronology

A Re-Os date must meet certain criteria if it is to be interpreted as a reliable age estimate, including: 1) the $^{187}Os/^{188}Os$ values of organic-rich shales within the same time frame are similar; 2) the Re-Os system must be closed at or soon after deposition; (3) a wide enough range of $^{187}Re/^{188}Os$ ratios is required in order to generate an equivalent range of present day $^{187}Os/^{188}Os$; and (4) the Re and Os within the sample are hydrogenous in origin. The MSWD calculated from the regression data is greater than unity. This may be the result of the $^{187}Os/^{188}Os$ ratios of contemporaneous samples were not similar, or that the Re-Os system was not closed at the time of deposition. Regardless, some first-order interpretations can be made using these data. The biostratigraphic age determined via the correlation of shelf fusulinids (299-309 Ma; Waite et al., 2015) to basinal deposits falls within the error of the Re-Os age (300 ± 18 Ma). The initial $^{187}Os/^{188}Os$ value of 0.66 calculated from the regression is significantly lower than the $^{187}Os/^{188}Os$ value for present day seawater, and likely reflects the $^{187}Os/^{188}Os$ ratio of the seawater at the time of deposition. The high MSWD is a key constraint on the precision of the Re-Os data, and indicates scatter due to geologic processes. Molybdenum enrichment factors within the Midland Basin suggest that there was a redox gradient along strike during the Late Pennsylvanian from north to south. Different rates of recharge or mixing could potentially affect the initial $^{187}Os/^{188}Os$ ratio such that contemporaneous samples do not have identical values. Other causes that may alter the $^{187}Os/^{188}Os$ ratio include thermal maturation of hydrocarbons, metamorphism of the black mudrock, and meteoritic/detrital sources of Os (Cohen et al., 1999; Creaser et al., 2003; Kendall et al., 2004).

Measurements of the temperature at depth recorded during drilling reached a maximum of 172 ^{o}F, which is too low for fractionation of Re and Os to occur (Kendall et al., 2004). This is also supported by the observation that no evidence of metamorphism was found within the core. Even if metamorphism had occurred, the data collected could still potentially be used. Black shales from Western Canada that had undergone chlorite grade metamorphism, ~300-400 ^{o}C, were dated geochronologically using the Re-Os system (Kendall et al., 2004). It was determined that perturbation of Re-Os systematics due to metamorphism was either not detected, or unobservable at the scale that samples were collected. It is therefore interpreted that alteration of the Re and Os composition due to metamorphism is not a valid explanation for the large MSWD.

Cosmogenic osmium from meteorites could induce error into the age measurement as a non-hydrogenous Os. Unfortunately, no quantitative measurements of the meteoritic flux during the Pennsylvanian have been conducted. If the flux is comparable to that during the Cenozoic, then it can be assumed that its impact is negligible (Cohen et al., 1999; Kendall et al., 2004). Peucker-Ehrenbrink (1996) calculated the Cenozoic flux of Os by studying pelagic sediments collected from the Pacific Ocean. If the meteoritic input is approximately 3.7×10^{4} T/yr, and a chondritic meteorite has an Os abundance of 486 ppb, a sediment accumulation rate of 50 m/Ma yields a cosmogenic Os flux of 0.28×10^{-12} g Os/g (Peucker-Ehrenbrink, 1996; Cohen et al., 1999; Kendall et al., 2004). The average Os concentration of the Midland Basin samples is 1.172 ppb (n=5). Assuming that the meteoritic flux from the Cenozoic is similar to the flux during the Pennsylvanian, then cosmogenic Os accounts for ~0.023%

of the total Os budget and can therefore be also be discounted as a potentially confounding factor in the age determination (Cohen et al., 1999; Kendall et al., 2004).

Detrital osmium is a potential source of error within the Re-Os dates. Mixing detrital Os with hydrogenous Os components could result in an age that is not indicative of the depositional age. Detrital Os has been shown to impact Re-Os age dates in black shales from the Exshaw Formation in Alberta, Canada (Selby and Creaser, 2003). Small variations were found in the ages when using two different methods for preparing the samples for analysis, inverse aqua regia and CrO_3-H_2SO_4 digestions. Both calculated ages fall within the known stratigraphic ages of the formation (634 ± 57 Ma, MSWD=65; and 607.8 ± 4.7 Ma. MSWD=1.2, respectively) (Kendall et al., 2004). However, the date obtained via the inverse aqua regia has a larger error and higher MSWD compared to the CrO_3-H_2SO_4 method (Figure 5.3). Those authors attributed this discrepancy to the inverse aqua regia method dissolving detrital (non-hydrogenous) Os. This can be a significant factor in determining the depositional age of a black shale, as the presence of detrital Os has been proven to affect the Re-Os systematics within black shales (Selby and Creaser, 2003; Kendall et al., 2004). Kendall et al. (2004) suggested that if the input of detrital osmium into the system is constant, then the effect would be stronger in black shales with low TOC content, approximately < 2.0%. This is due to low TOC shales containing relatively low concentrations of Re and Os as well. While the C:N ratios demonstrate that most of the organic matter is composed of alginite, and therefore hydrogenous in origin, Selby and Creaser (2003) suggest that >60% detrital Os is required to affect the Re-Os systematics. The proportion of unradiogenic (non-hydrogenous) Os relative to radiogenic Os is unknown. The samples selected for the Re-Os analysis all contain greater than 5%

TOC (6.06%, 8.95%, and 5.05%, for Martin, Midland, and Upton counties, respectively), and the abundances of Re and Os are in the range of parts per billion (ppb) each, while other studies report Re in ppb and Os in parts per trillion (ppt). Therefore, by this criteria, the abundances of Re and Os from Midland Basin are more than adequate for dating via the Re-Os geochronometer. The age calculated using the Re-Os geochronometer is interpretable as an absolute age, as it is in agreement with previous biostratigraphic correlations. However, we suggest that more study is needed before deterministically assigning the age to the WC-D due to the high MSWD from either non-hydrogenous Os or mixing within the basin.

5.4 Petroleum Geology

Understanding the depositional history WC-D is key to determining its potential as an unconventional petroleum play. While depositional history is not the only variable in defining the reservoir quality, knowledge of the inorganic and organic geochemistry and the stratigraphy can provide great insight. Key horizons that would provide the best hydrocarbon recovery are based on organic content, elemental geochemistry, and thickness, all of which are factors in determining the response an interval may have to hydraulic fracturing. Hydrocarbon reservoir potential is directly impacted by the organic enrichment of the interval in question, and the fracability is impacted by the inorganic geochemistry (Passey et al., 2010; Sone and Zoback, 2013). Black Mudrock 1 is interpreted to be the facies with the highest potential as an unconventional hydrocarbon reservoir in the WC-D, because of its high %Si, low %Al, and high TOC. Black Mudrock 2 contains higher %Al and %K, with lower TOC on average, potentially driving more

plastic/ductile behavior under induced stress compared to BMR-1 (Passey et al., 2010; Sone and Zoback, 2013). These differences in geochemistry result in BMR-1 to likely be the superior choice for target horizons. One complication is that BMR-1 beds are typically sandwiched between thicker BMR-2 packages, thus potentially making horizontal well completions more difficult.

Analyses conducted by Fischer and Warpinski (2013) determined that hydraulic fractures grow parallel to the direction of maximum stress and perpendicular to the direction of minimum stress. Micro-deformation measurements illustrate that at depths below 4,000 ft, the majority of fractures that propagate are vertical, and above 4,000 ft fractures are predominantly horizontal. Interlayering of strong and weak layers of varying lithology can hinder fracture propagation, preventing larger vertical fractures forming across complex stratigraphy (Fischer and Warpinski, 2013). As a result, fractures of the WC-D will most likely propagate vertically until reaching a change in lithology. This is an important consideration, due to the WC-D exhibiting high variability in lithology within some intervals, for example in the Middle WC-D.

Keeping these considerations in mind, two potential intervals for exploration of BMR-1 beds have been identified. The Upper WC-D contains the highest proportion of BMR-1 facies in the Martin County core. There are three potential horizons, but they are not continuous and separated by GMR and GRST facies. The Middle WC-D is the second, most abundant interval with respect to BMR-1 facies. Issues may stem from drilling the Middle WC-D, as it is also the interval with the highest variability in facies types. If BMR-2 facies are deemed acceptable targets for horizontal drilling, more options become available. The Lower WC-D contains a thick interval of BMR-2

interbedded with thin GMR beds. The WC-C2 is dominated by BMR-2 facies, but these horizons are finely interbedded with GMR, BMR-1, and GRST layers. The trade-off between targeting continuous beds of low TOC BMR-2 versus isolated BMR-1 intervals that are interlayered with variable facies requires additional research.

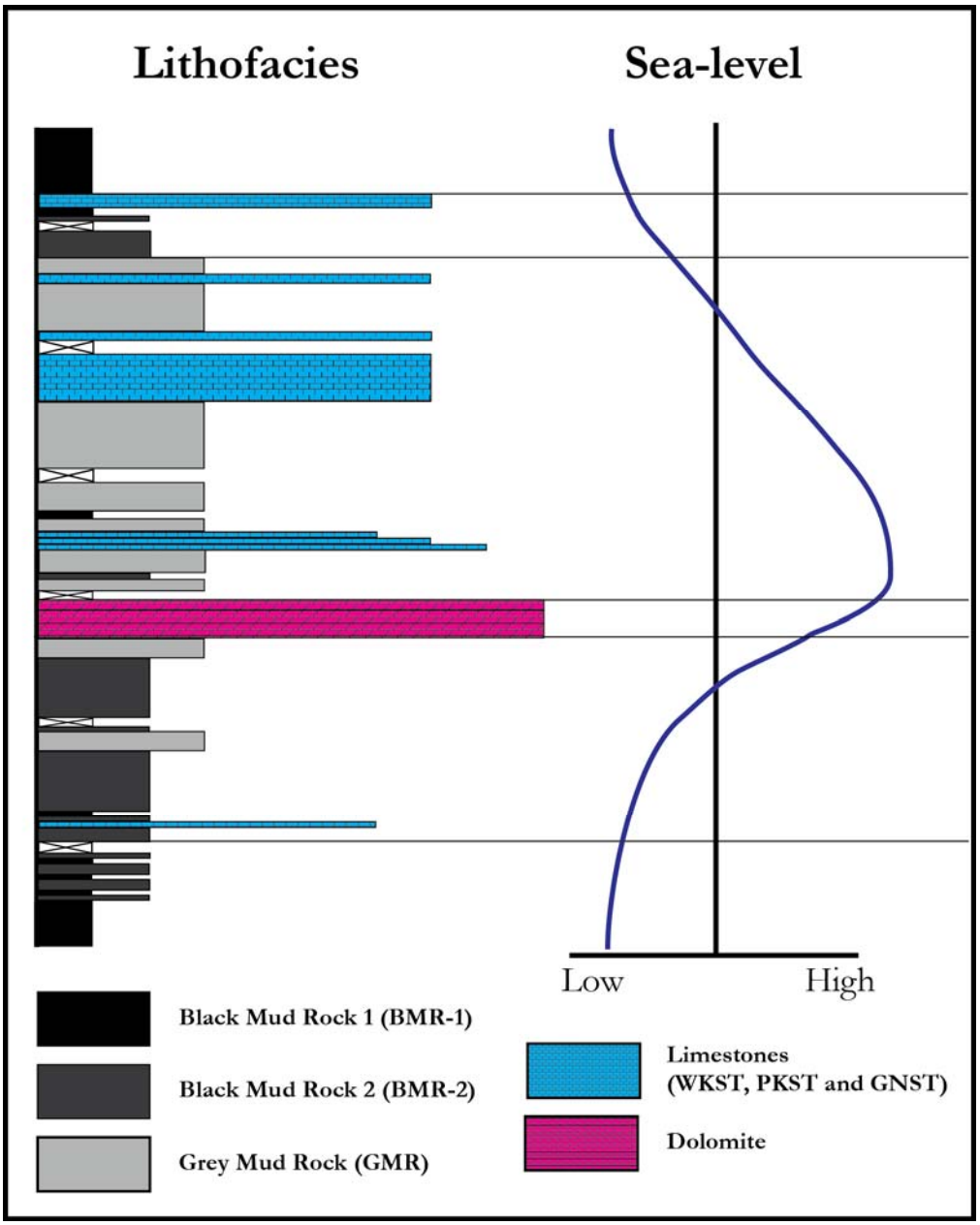

Figure 5.1 Type cycle for the Middle WC-D.
Cycles start from the base of a BMR-1 bed to the base of the next BMR-1 bed. Thin occurrences of BMR-1 are discounted as either the beginning or end of a cycle. Facies are tied to intervals of the sea level curve: BMR-1 represent maximum lowstand; BMR-2 for rising sea level; DOL are indicative of maximum rate of sea level rise; GMR and limestones represent highstands and early falling stage; BMR-2 for late stage regressions.

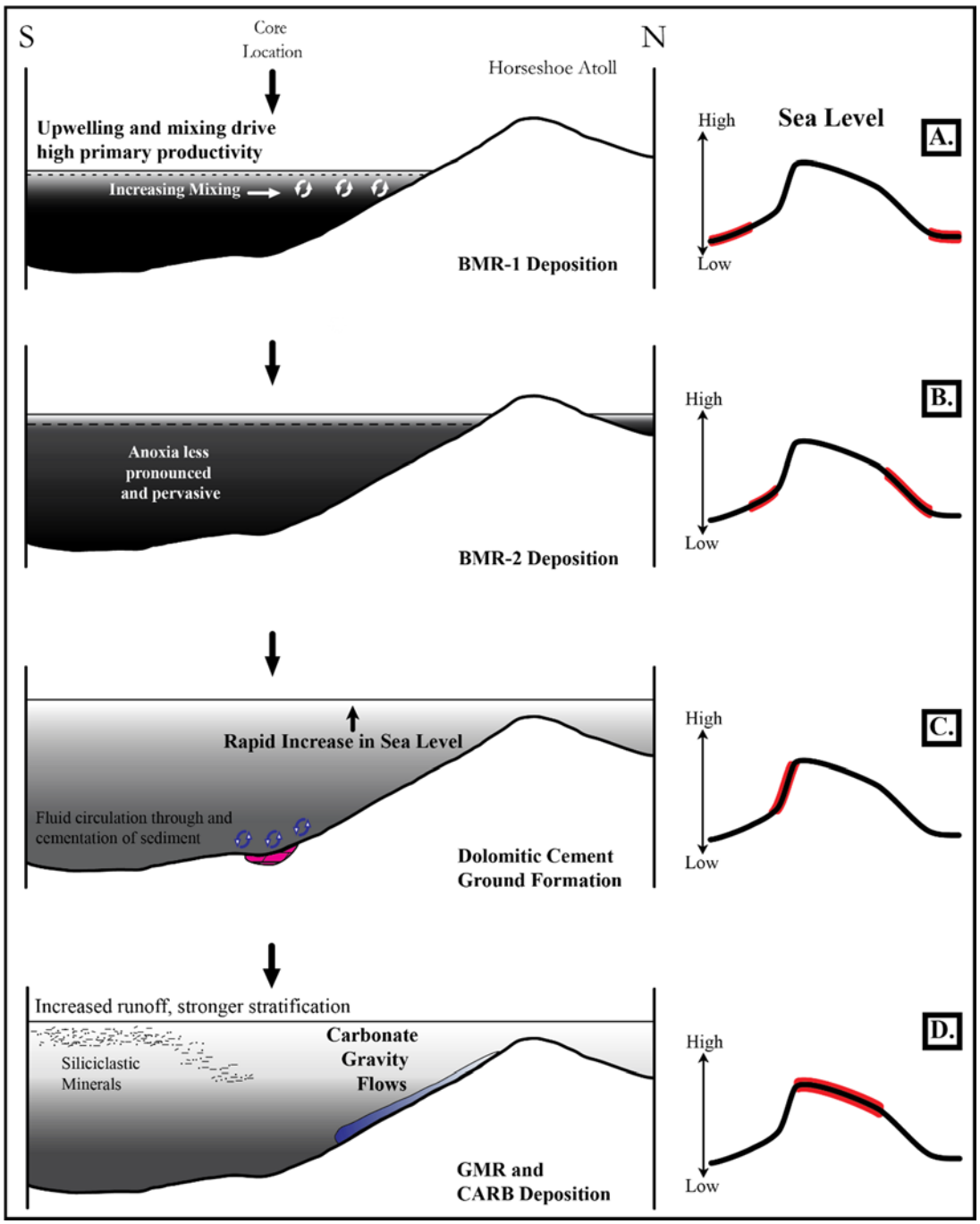

Figure 5.2 Schematic Depositional Model for the Wolfcamp D
(A) Lowstand deposition of BMR-1 facies during lowstand. Organic enrichment is driven by primary productivity due to upwelling. (B) BMR-2 deposition records a modest sea level rise and increase in continental runoff, reducing the impact of anoxia. (C) DOL deposition indicates maximum rate of sea level rise, sedimentation is at its lowest. (D) Shedding of siliciclastics and carbonate allochems due to increases runoff and high sea level shedding result in the deposition of GMR and CARB facies. Freshwater runoff strengthens stratification of the water column.

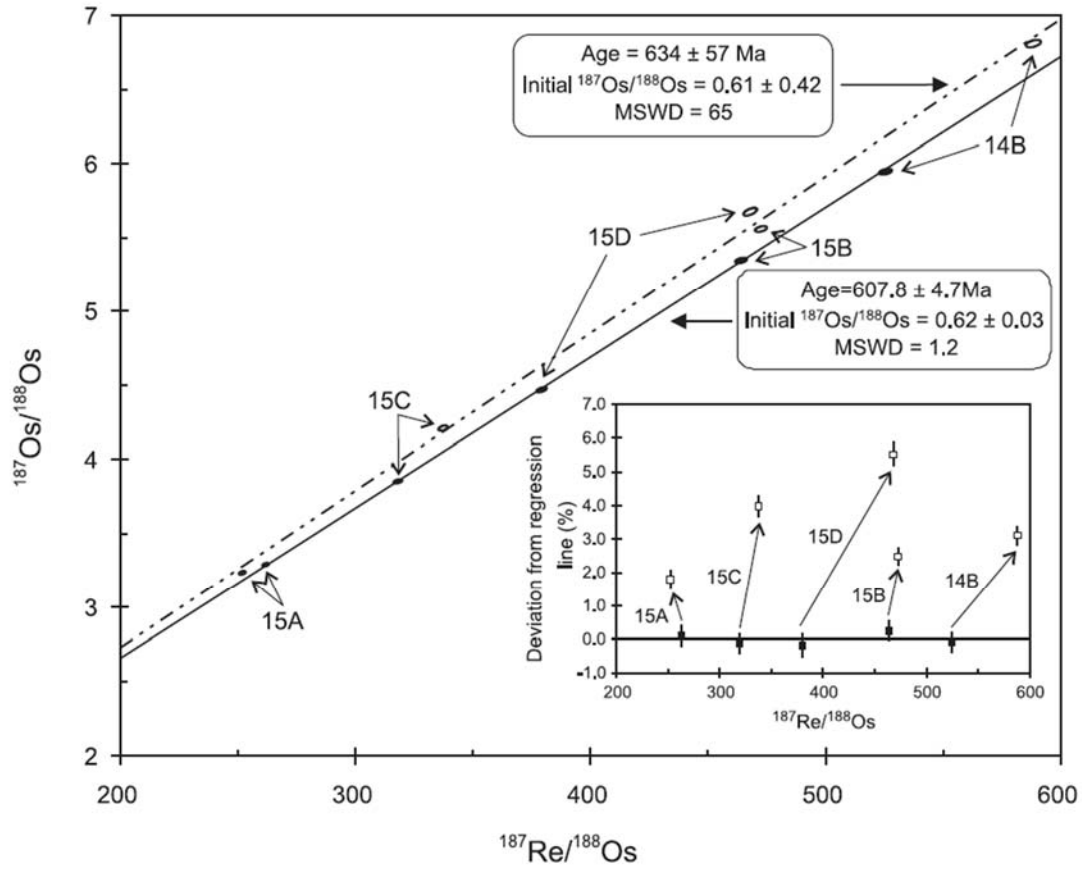

Figure 5.3 Comparison of inverse aqua regia and CrO_3-H_2SO_4 mudrock digestion methods. The open ellipses are analyses performed using the inverse aqua regia; the regression of these data is the dashed isochron line. CrO_3-H_2SO_4 analyses are indicated by closed ellipses and the solid regression line. The inset graph shows the deviation of each point from the CrO_3-H_2SO_4 regression (from Kendall et al., 2004).

CHAPTER SIX: CONCLUSIONS

- The integrated approach adopted for this study resulted in a new understanding of the relationship between the environmental and oceanographic changes that impacted the deposition of the WC-D in Martin County. This thesis aimed to test the hypothesis that the stratigraphic development of the WC-D was strongly influenced by glacioeustatic sea level change, as well as to test the hypothesis that the depositional age of the WC-D is Late Pennsylvanian by using Re-Os geochronology. The Re-Os date of 300 ± 18 Ma (MSWD = 63) holds several assumptions if the date is interpreted to be geologically significant: (1) the initial $^{187}Os/^{188}Os$ values of BMR-1 samples are similar; (2) the Re-Os system was closed at or subsequently following deposition; (3) a wide enough range of $^{187}Re/^{188}Os$ ratios is required in order to generate an appropriate range of current $^{187}Os/^{188}Os$ values; and (4) the Re and Os within the sample are hydrogenous in origin. Reasons for why the MSWD is above unity are potentially tied to the first assumption. Detrital osmium is most likely a source of error within the Re-Os measurement. The aqua regia method of acid dissolution can dissolve detrital organic matter, thereby releasing Os of varying ages. This may explain why the MSWD is much greater than unity.

- The nine facies were identified based on geochemical, sedimentological, and petrographic properties, all which are tied to depositional processes. Three are varying types of mudrocks with differences in geochemistry: (1) Black Mudrock 1 (BMR-1); Black Mudrock 2 (BMR-2); and (3) Gray Mudrock (GMR). Four consist of carbonate lithologies: (1) Wackestones (WKST); (2) Packstones (PKST); (3) Grainstones (GRST); and (4) Dolomitized cement grounds (DOL). The eighth and ninth facies, mixed and

diagenetic mineral types, were was also identified but do not represent a large volume of core compared to the Upton County core (Baldwin, 2016).

- We interpret depositional cycles linked to sea level change in the Martin County core. Type cycles in the Martin County core consists of (moving up-section): BMR-1; BMR-2; GMR (+/- WKST, PKST, GNST, DOL); BMR-2; and BMR-1. While not all cycles exhibit every facies type, this general pattern is repetitive throughout the core. Long term trends can be seen in the stacking patterns, facies abundances, and geochemistry, moving from stratigraphically low to high. These shifts are likely the result of sea level fluctuating during the Late Pennsylvanian, and allow for the separation of the WC-D into the three subintervals: Lower, Middle, and Upper WC-D.
- Within the three intervals of the WC-D, there are multiple sea level cycles based on the changes in facies stacking patterns. Eleven sea level cycles were interpreted for the WC-D. Other studies with high resolution age control have demonstrated by using time series analysis that cyclothem development is largely driven by the Earth's eccentricity (Rasbury et al., 1988; van den Belt et al., 2015). Most studies of cyclothems were conducted in either shelf environments (the U.S. Midcontinent) or in transitional marine environments with high terrigenous inputs (eastern Kentucky). This study is among the first of its kind to identify cyclothems in a restricted basin environment.
- The high organic content and petroleum source rock potential of BMR-1 facies is likely a function of: (a) high primary productivity, perhaps influenced by upwelling; (b) favorable preservation of organic matter on the sea floor due to redox conditions; and (c) limited siliciclastic or carbonate dilution. This interpretation is supported by elevated %Si content, which petrography has revealed to be biogenic in

origin, filling *Tasmanites* cysts. Low Mo/TOC ratios suggest that bottom water recharge rates were low and anoxia was pervasive during deposition. Molar carbon-to-nitrogen ratios imply that most of the organic matter within the WC-D is derived from marine sources, with average values within the range of 10-15. The predominant maceral type is alginite, which is consistent with the C:N ratio interpretation of the organic matter being marine in origin. Carbon-to-nitrogen molar ratios greater than 10-15 are potentially the result of denitrification in anoxic marine environments (Algeo et al., 2008).

- Classic models of sequence stratigraphy for mixed siliciclastic and carbonate systems predict that the shedding of allocthonous carbonate materials towards the basin center occurs during sea level highstands. Gray mudrock packages, along with WKST, PKST, and GRST intervals, represent an increase in carbonate allochems transported from up-dip via gravity flows. Dolomitized cement grounds formed *in situ* when sea level rise was at its maximum rate and the basin was starved in siliciclastic sediment. Black Mudrock 2 facies are interpreted to be a transitional facies, between BMR-1 and GMR facies types, and indicate times of early sea level transgression or late-stage sea level regression.

- The goal of developing an unconventional reservoir is to artificially induce fractures and recover hydrocarbons. High TOC, optimal interval thickness, brittleness, and formation integrity are important characteristics of potential horizontal landing zones. We interpret that BMR-1 facies has strong potential as an unconventional petroleum source rock, due to its high TOC content and high %Si, which could make it amenable to hydraulic fracturing. The results of this study indicate that unlike Upton and Midland counties, Upper WC-D is a strong potential target for WC-D wells, with the

Middle WC-D as a secondary objective. This is due to the relatively high abundance of organic-rich BMR-1 within the Upper WC-D.

REFERENCES

Al-Awadi, M., Clark, W.J., Moore, W.R., Herron, M., Zhang, T., Zhao, W., Hurley, N., Kho, D., Montaron, B., and Sadooni, F., 2009, Dolomite: Perspectives on a Perplexing Mineral, Oilfield Review, Autumn, v. 21, no. 3.

Algeo, T.J., and Heckel, P.H., 2008, The Late Pennsylvanian Midcontinent Sea of North America : A review: Palaeogeography, Palaeoclimatology, Palaeoecology, v. 268, no. 3–4, p. 205–221.

Algeo, T.J., and Maynard, J.B., 2004, Trace-element behavior and redox facies in core shales of Upper Pennsylvanian Kansas-type cyclothems: Chemical Geology, v. 206, no. 3–4, p. 289–318.

Algeo, T.J., and Rowe, H., 2012, Paleoceanographic applications of trace-metal concentration data: Chemical Geology, v. 324–325, p. 6–18.

Alves, T.M., 2015, Submarine slide blocks and associated soft-sediment deformation in deep-water basins: A review: Marine and Petroleum Geology, v. 67, p. 262–285.

Atchley, S.C., Kozar, M.G., and Yose, L.A., 1999, A Predictive Model for Reservoir Distribution in the Permian (Leonardian) Clear Fork and Glorieta Formations, Robertson Field Area, West Texas: AAPG Bulletin, v. 83, no. 7, p. 1031–1055.

Benson, D.J., 1985, Depositional history of the Smackover Formation in southwest Alabama: GCAGS Transactions, v. 38, p. 197–205.

Boardman, D.R., and Heckel, P.H., 1989, Glacial-eustatic sea-level curve for early Late Pennsylvanian sequence in north-central Texas and biostratigraphic correlation with curve for midcontinent North America: Geology, v. 17, no. 9, p. 802–805.

Bohacs, K.M., 1990, Sequence stratigraphy of the Monterey Formation, Santa Barbara County: Integration of physical, chemical, and biofacies data from outcrop and subsurface, *in* SEPM, Core Workshop 14, p. 139–200.

Bohacs, K. et al., 2014, Parasequence types in shelfal mudstone strata — Quantitative observations of lithofacies and stacking patterns , and conceptual link to modern depositional regimes: Geology, v. 42, no. 2, p. 6–10.

Clark, P.U., Alley, R.B., and Pollard, D., 1999, Northern Hemisphere ice-sheet influences on global climate change: Science, v. 286, no. 5442, p. 1104–1111.

Cohen, A.S., Coe, A.L., Bartlett, J.M., and Hawkesworth, C.J., 1999, Precise Re-Os ages of organic-rich mudrocks and the Os isotope composition of Jurassic seawater: Earth and Planetary Science Letters, v. 167, no. 3–4, p. 159–173.

Dunham, R.J., 1962, Classification of Carbonate Rocks According to Depositional Texture, *in* M 1: Classification of Carbonate Rocks - A Symposium, p. 108–121.

Eros, J.M., Montañez, I.P., Davydov, V.I., Osleger, D.A., Nemyrovska, T.I., Poletaev, V.I., and Zhykalyak, M. V., 2012, Reply to the comment on: "Sequence stratigraphy and onlap history of the Donets Basin, Ukraine: Insight into Carboniferous icehouse dynamics": Palaeogeography, Palaeoclimatology, Palaeoecology, v. 363–364, p. 187–191.

Esposito Jr., R.A., and King Jr., D.T., 1987, Facies analysis, sea-level history, and platform evolution of the Jurassic Smackover Formation, Conecuh Basin, Escambia County, Alabama: Transactions of the Gulf Coast Association of Geological Societies, v. 37, p. 335–346.

Esser, B.K., and Turekian, K.K., 1993, The osmium isotopic composition of the continental-crust: Geochim. Cosmochim. Acta, v. 57, no. 13, p. 3093–3104.

Ettensohn, F.R., Miller, M.L., Dillman, S.B., Elam, T.D., Geller, K.L., Swager, D.R., Markowitz, G., and Barron, L.S., 1988, Characterization and implications of the Devonian-Mississippian black shale sequence, eastern and central Kentucky, U.S.A.: pycnoclines, transgression, regression, and tectonism: Canadian Society of Petroleum Geologists Memoir, v. 14, p. 323–345.

Fielding, C.R., Frank, T.D., Birgenheier, L.P., Rygel, M.C., Jones, a. T., and Roberts, J., 2008, Stratigraphic imprint of the Late Palaeozoic Ice Age in eastern Australia: a record of alternating glacial and nonglacial climate regime: Journal of the Geological Society, v. 165, no. 1, p. 129–140.

Fielding, C.R., Frank, T.D., and Isbell, J.L., 2008, The late Paleozoic ice age-A review of current understanding and synthesis of global climate patterns: Geological Society of America Special Papers, v. 441, no. January, p. 343–354.

Fisher, K., and Warpinski, N., 2012, Hydraulic-Fracture-Height Growth : Real Data: SPE Productions & Operations, v. 1, no. February, p. 8–19.

Frenzel, H.N., and et al., 1988, The Permian Basin Region, *in* Sloss, L. ed., The Geology of North America, Vol. D-2, Sedimentary Cover - North American Craton U.S., The Geological Society of America, p. 261–306.

Galley, J., 1958, Oil And Geology In The Permian Basin Of Texas And New Mexico: SP 18: Habitat of Oil, p. 395–446.

Gaswirth, S.B., Marra, K.R., Lillis, P.G., Mercier, T.J., Leathers-Miller, H.M., Schenk, C.J., Klett, T.R., Le, P.A., Tennyson, M.E., Hawkins, S.J., Brownfield, M.E.,

Pitman, J.K., and Finn, T.M., 2016, Assessment of undiscovered continuous oil resources in the Wolfcamp shale of the Midland Basin, Permian Basin Province, Texas: U.S. Geological Survey Fact Sheet, v. 2016–3092, no. November.

Gaswirth, S., Marra, K., Cook, T., Charpentier, R.R., Gautier, D.L., Higley, D.K., Klett, T.R., Lewan, M.D., Lillis, P.G., Schenk, C.J., Tennyson, M.E., and Whidden, K.J., 2013, Assessment of Undiscovered Oil Resources in the Bakken and Three Forks Formations, Williston Basin Province, Montana, North Dakota, and South Dakota: USGS Fact Sheet, , no. April, p. 1–4.

Greb, S.F., Pashin, J.C., Martino, R.L., and Eble, C.F., 2008, Appalachian sedimentary cycles during the Pennsylvanian: Changing influences of sea level, climate, and tectonics: Resolving the Late Paleozoic Ice Age in Time and Space, v. 441, no. January, p. 235–248.

Hamlin, S.H., and Baumgardner, R.W., 2012, Wolfberry (Wolfcampian-Leonardian) Deep-water Depositional Systems in the Midland Basin: Stratigraphy, Lithofacies, Reservoirs, and Source Rocks.

Heavens, N.G., Mahowald, N.M., Soreghan, G.S., Soreghan, M.J., and Shields, C.A., 2015, A model-based evaluation of tropical climate in Pangaea during the late Palaeozoic icehouse: Palaeogeography, Palaeoclimatology, Palaeoecology, v. 425, p. 109–127.

Heckel, P.H., 1986, Sea-level curve for Pennsylvanian eustatic marine transgressive-regressive depositional cycles along midcontinent outcrop belt, North America: Geology, v. 14, p. 330–334.

Heckel, P.H., 2008, Pennsylvanian cyclothems in Midcontinent North America as far-field effects of waxing and waning of Gondwana ice sheets: Geological Society of America Special Papers, v. 441, no. 303, p. 275–289.

Hobson, J.P., Caldwell, C.D., and Toomey, D.E., 1985, Early Permian Deep-Water Allochthonous Limestone Facies and Reservoir, West Texas: AAPG Bulletin, v. 69, no. 12, p. 2130–2147.

Hoffman, D., Algeo, T., JB, M., Joachimski, M., Hower, J., and Jaminski, J., 1998, Regional and stratigraphic variation in bottomwater anoxia in offshore core shales of Upper Pennsylvanian Cyclothems from the Eastern Midcontinent Shelf (Kansas), U.S.A.: Shales and Mudstones, v. 1, no. January 2017, p. 243–269.

Horton, D.E., Poulsen, C.J., Montañez, I.P., and DiMichele, W.A., 2012, Eccentricity-paced late Paleozoic climate change: Palaeogeography, Palaeoclimatology, Palaeoecology, v. 331–332, p. 150–161.

Isbell, J.L., Henry, L.C., Gulbranson, E.L., Limarino, C.O., Fraiser, M.L., Koch, Z.J., Ciccioli, P.L., and Dineen, A.A., 2012, Glacial paradoxes during the late Paleozoic ice age: Evaluating the equilibrium line altitude as a control on glaciation: Gondwana Research, v. 22, no. 1, p. 1–19.

Jacobs, T., 2013, Cracking the Cline: A New Shale Play Develops in the Permian basin: Journal of Petroleum Technology, p. 70–77.

Jaminski, J., Algeo, T.J., Maynard, J.B., Hower, J.C., 1998, Climatic Origin of dm-Scale Compositional Cyclicity in the Cleveland Member of the Ohio Shale (Upper Devonian), Central Appalachian Basin, U.S.A.: Shales and Mudstones, v. 1, p. 217–242.

Jarvie, D.M., Hill, R.J., Ruble, T.E., and Pollastro, R.M., 2007, Unconventional shale-gas systems: The Mississippian Barnett Shale of north-central Texas as one model for thermogenic shale-gas assessment: AAPG Bulletin, v. 91, no. 4, p. 475–499.

Kendall, B.S., Creaser, R. a., Ross, G.M., and Selby, D., 2004, Constraints on the timing of Marinoan "Snowball Earth" glaciation by 187Re-187Os dating of a Neoproterozoic, post-glacial black shale in Western Canada: Earth and Planetary Science Letters, v. 222, no. 3–4, p. 729–740.

Loucks, R.G., and Sarg, J.F., 1983, Carbonate Sequence Stratigraphy: Recent Developments and Applications, AAPG Memoir 57: AAPG.

Ludwig, K.R., 2008, User's Manual for Isoplot 3.70: A Geochronological Toolkit for Microsoft Excel: Berkeley Geochronology Center Special Publication, no. 4, p. 76.

Mazzullo, S., and Reid, A., 1989, Lower Permian Platform and Basin Depositional Systems, Northern Midland Basin, Texas: SEPM Special Publication, no. 44, p. 305–320.

Montañez, I.P., and Poulsen, C.J., 2013, The Late Paleozoic Ice Age: An Evolving Paradigm: Annual Review of Earth and Planetary Sciences, v. 41, no. 1, p. 629–656.

Nier, A.O., 1950, A redetermination of the relative abundances of the isotopes of carbon, nitrogen, oxygen, argon, and potassium: Physical Review, v. 77, no. 6, p. 789–793.

Passey, Q.R., Bohacs, K.M., Esch, W.L., Klimentidis, R., Sinha, S., and Upstream, E., 2010, From Oil-Prone Source Rock to Gas-Producing Shale Reservoir – Geologic and Petrophysical Characterization of Unconventional Shale-Gas Reservoirs: CPS/SPE International Oil & Gas Conference and Exhibition in China 2010, p. 1707–1735.

Posamentier, H.W., and Walker, R.G., 2006, Deep-Water Turbidites and Submarine Fans, *in* Posamentier, H.W. and Walker, R.G. eds., Facies Models Revisited, p. 399–520.

Rasbury, E.T., Hanson, G.N., Meyers, W.J., Holt, W.E., Goldstein, R.H., and Saller, A.H., 1998, U-Pb dates of paleosols: constraints on late Paleozoic cycle durations and boundary ages: Geology, v. 26, no. 5, p. 403–406.

Rasoazanamparany, C., Widom, E., Siebe, C., Guilbaud, M.N., Spicuzza, M.J., Valley, J.W., Valdez, G., and Salinas, S., 2016, Temporal and compositional evolution of Jorullo volcano, Mexico: Implications for magmatic processes associated with a monogenetic eruption: Chemical Geology, v. 434, p. 62–80.

Ring, E.J., 1993, the Preparation and Certification of Fourteen South African Silicate Rocks for Use As Reference Materials: Geostandards Newsletter, v. 17, no. 1, p. 137–158.

Ross, C.A., and Ross, J.R.P., 1987, Late Paleozoic sea levels and depositional sequences, in Ross, C.A., and Haman, D., eds., Timing and depositional history of eustatic sequences: Constraints on seismic stratigraphy: Cushman Foundation for Foraminiferal Research, , no. 24, p. 137–149.

Rowe, H., Hughes, N., and Robinson, K., 2012, The quantification and application of handheld energy-dispersive x-ray fl uorescence (ED-XRF) in mudrock chemostratigraphy and geochemistry: Chemical Geology, v. 324–325, p. 122–131.

Rygel, M.C., Fielding, C.R., Frank, T.D., and Birgenheier, L.P., 2008, The Magnitude of Late Paleozoic Glacioeustatic Fluctuations: A Synthesis: Journal of Sedimentary Research, v. 78, no. 8, p. 500–511.

Sageman, B.B., Murphy, A.E., Werne, J.P., Ver, C.A., Hollander, D.J., and Lyons, T.W., 2003, A tale of shales: the relative roles of production, decomposition, and dilution in the accumulation of organic-rich strata, Middle – Upper Devonian, Appalachian basin: Chemical Geology, v. 195, p. 229–273.

Saller, A.H., Dickson, J.A.D., Rasbury, E.T., Ebato, T., 1999, Effects of Long-Term Accomodation Change on Short-Term Cycles, Upper Paleozoic Platform Limestones, West Texas: SEPM Special Publication, no. 63, p. 227–246.

Saller, A.H., Dickson, J.A.D., and Boyd, S.A., 1994, Cycle stratigraphy and porosity in Pennsylvanian and Lower Permian shelf limestones, eastern Central Basin platform, Texas: American Association of Petroleum Geologists Bulletin, v. 78, no. 12, p. 1820–1842.

Sanders, J.E., 1960, Primary Sedimentary Structures Formed By Turbidity Currents and Related Resedimentation Mechanisms: The Society of Economic Paleontologists and Mineralogists, v. SP12, p. 192–219.

Schieber, J., 1996, Early Diagenetic Silica Deposition in Algal Cysts and Spores: A Source of Sand in Black Shales? Journal of Sedimentary Research, v. 66, no. 1, p. 175–183.

Schlager, W., 2005, Carbonate Sedimentology and Sequence Stratigraphy (L. J. Crossey, Ed.): SEPM.

Schlager, W., and Reijmer, J.J.G., 2009, Carbonate platform slopes of the Alpine Triassic and the Neogene - A comparison: Austrian Journal of Earth Sciences, v. 102, no. 1, p. 4–14.

Scott, C., and Lyons, T.W., 2012, Contrasting molybdenum cycling and isotopic properties in euxinic versus non-euxinic sediments and sedimentary rocks: Refining the paleoproxies: Chemical Geology, v. 324–325, p. 19–27.

Selby, D., and Creaser, R. a., 2003, Re-Os geochronology of organic rich sediments: An evaluation of organic matter analysis methods: Chemical Geology, v. 200, no. 3–4, p. 225–240.

Shanmugam, G., and Iii, G.L.B., 1978, Fine-grained Carbonate Debris Flow, Ordovician Basin Margin, Southern Appalachians: v. 48, no. 4, p. 1233–1239.

Shanmugam, G., 1997, The Bouma Sequence and the turbidite mind set: Earth-Science Reviews, v. 42, no. 4, p. 201–229.

Shirey, S.B., and Walker, R.J., 1998, Isotope System in Cosmochemistry and High-Temperature Geochemistry: Annual Review of Earth and Planetary Sciences, v. 26, no. 1, p. 423–500.

Shumaker, R.C., 1992, Paleozoic Structure of the Central Basin uplift and Adjacent Delaware Basin, West Texas: American Association of Petroleum Geologists Bulletin, v. 76, no. 11, p. 1804–1824.

Silva, A.J., and Booth, J.S., 1984, Creep behavior of submarine sediments: Geo-Marine Letters, v. 4, no. 3, p. 215–219.

Sloss, L., 1963, Sequences in the Cratonic Interior of North America: GSA Bulletin, v. 74, no. February, p. 93–114.

Sone, H., and Zoback, M.D., 2013, Mechanical properties of shale-gas reservoir rocks—Part 2: Ductile creep, brittle strength, and their relation to the elastic modulus: Geophysics, v. 78, no. 5, p. D393–D402.

Soreghan, G.S., 1994, The impact of glacioclimatic change on Pennsylvanian cyclostratigraphy: Canadian Society of Petroleum Geologists, v. 17, no. January 1994, p. 21.

Soreghan, G.S., and Giles, K.A., 1999, Amplitudes of late Pennsylvanian glacioeustasy: Geology, v. 27, no. 3, p. 255–258.

Soreghan, G.S., Sweet, D.E., and Heavens, N.G., 2014, Upland Glaciation in Tropical Pangaea: Geologic Evidence and Implications for Late Paleozoic Climate Modeling: The Journal of Geology, v. 122, no. 2, p. 137–163.

Tabor, N.J., and Poulsen, C.J., 2008, Palaeoclimate across the Late Pennsylvanian-Early Permian tropical palaeolatitudes: A review of climate indicators, their distribution, and relation to palaeophysiographic climate factors: Palaeogeography, Palaeoclimatology, Palaeoecology, v. 268, no. 3–4, p. 293–310.

Tribovillard, N., et al., 2006, Trace metals as paleoredox and paleoproductivity proxies : An update: Chemical Geology, v. 232, p. 12–32.

van den Belt, F.J.G., van Hoof, T.B., and Pagnier, H.J.M., 2015, Revealing the hidden Milankovitch record from Pennsylvanian cyclothem successions and implications regarding late Paleozoic chronology and terrestrial-carbon (coal) storage: Geosphere, v. 11, no. 4, p. 1062–1076.

Veevers, J.J., and Powell, C.M., 1987, Late Paleozoic glacial in Gondwanaland reflected in trangressive-regressive depostional sequences in Euramerica: Geological Society of America Bulletin, v. 98, no. April, p. 475–487.

Waite, L., and Read, T., 2014, Unraveling the Wolfcamp D interval in the Midland Basin: Initial Observations:

West, R.R., Archer, A.W., and Miller, K.B., 1997, The role of climate in stratigraphic patterns exhibited by late Paleozoic rocks exposed in Kansas: v. 128, p. 1–16.

Yang, K.-M., and Dorobek, S.L., 1995, The Permian Basin of West Texas and New Mexico: Tectonic History of a “Composite” Foreland Basin and its Effects on Stratigraphic Development: SEPM Special Publication, no. 52, p. 149–174.

VITA

Zachary Seth Perlman

Education

B.S. Geosciences (2012)

Denison University

Experience

Graduate Research Assistant

Pioneer Paleoenvironments and Stratigraphy Lab

Department of Earth and Environmental Sciences

University of Kentucky, 40506

Graduate Teaching Assistant

Department of Earth and Environmental Sciences

University of Kentucky, 40506

Physical Scientist

United States Geological Survey

Denver, Colorado, 80225